

This discussion paper is/has been under review for the journal Atmospheric Chemistry and Physics (ACP). Please refer to the corresponding final paper in ACP if available.

Constraining firm diffusivity

C. M. Trudinger et al.

How well do different tracers constrain the firm diffusivity profile?

C. M. Trudinger¹, I. G. Enting², P. J. Rayner³, D. M. Etheridge¹, C. Buizert^{4,5}, M. Rubino^{1,4}, P. B. Krummel¹, and T. Blunier⁴

¹Centre for Australian Weather and Climate Research, CSIRO Marine and Atmospheric Research, Aspendale, Victoria, Australia

²MASCOS, University of Melbourne, 3010, Victoria, Australia

³School of Earth Sciences, University of Melbourne, 3010, Victoria, Australia

⁴Centre for Ice and Climate, Niels Bohr Institute, University of Copenhagen, Juliane Maries vej 30, 2100 Copenhagen, Denmark

⁵College of Earth, Ocean, and Atmospheric Sciences, Oregon State University, Corvallis OR 97331, USA

Received: 24 June 2012 – Accepted: 4 July 2012 – Published: 19 July 2012

Correspondence to: C. M. Trudinger (cathy.trudinger@csiro.au)

Published by Copernicus Publications on behalf of the European Geosciences Union.

Title Page

Abstract

Introduction

Conclusions

References

Tables

Figures

◀

▶

◀

▶

Back

Close

Full Screen / Esc

Printer-friendly Version

Interactive Discussion



Abstract

Firn air transport models are used to interpret measurements of the composition of air in firn and bubbles trapped in ice in order to reconstruct past atmospheric composition. The diffusivity profile in the firn is usually calibrated by comparing modelled and measured concentrations for tracers with known atmospheric history. However, in some cases this is an under-determined inverse problem, often with multiple solutions giving an adequate fit to the data (this is known as equifinality). Here we describe a method to estimate the firn diffusivity profile that allows multiple solutions to be identified, in order to quantify the uncertainty in diffusivity due to equifinality. We then look at how well different combinations of tracers constrain the firn diffusivity profile. Tracers with rapid atmospheric variations like CH_3CCl_3 , HFCs and $^{14}\text{CO}_2$ are most useful for constraining molecular diffusivity, while $\delta^{15}\text{N}_2$ is useful for constraining parameters related to convective mixing near the surface. When errors in the observations are small and Gaussian, three carefully selected tracers are able to constrain the molecular diffusivity profile well with minimal equifinality. However, with realistic data errors or additional processes to constrain, there is benefit to including as many tracers as possible to reduce the uncertainties. We calculate CO_2 age distributions and their spectral widths with uncertainties for five firn sites (NEEM, DE08-2, DSSW20K, South Pole 1995 and South Pole 2001) with quite different characteristics and tracers available for calibration. We recommend moving away from the use of a single firn model with one calibrated parameter set to infer atmospheric histories, and instead suggest using multiple parameter sets, preferably with multiple representations of uncertain processes, to allow quantification of the uncertainties.

1 Introduction

Firn is the porous layer of compacted snow overlying an ice sheet. Air is contained in the open pores, and its composition is influenced by changes in the composition of the

ACPD

12, 17773–17834, 2012

Constraining firn diffusivity

C. M. Trudinger et al.

Title Page

Abstract

Introduction

Conclusions

References

Tables

Figures

◀

▶

◀

▶

Back

Close

Full Screen / Esc

Printer-friendly Version

Interactive Discussion



overlying atmosphere and by processes that occur in the firn. Air can be extracted from the firn and its composition measured (Schwander et al., 1993), providing an archive of old air from which to deduce the atmospheric histories and budgets of key gases. Firn is also the path that is traversed by air before being trapped into bubbles in ice. It is for both of these reasons that we are interested in the firn processes, which include advection downwards as new snow falls at the surface, convective mixing due to wind pumping near the surface (Colbeck, 1989; Severinghaus et al., 2001; Kawamura et al., 2006), molecular diffusion through the firn column (Schwander et al., 1988), enrichment of heavier molecules with depth due to gravitational settling (Craig et al., 1988; Schwander, 1989), thermal fractionation due to temperature gradients (Severinghaus et al., 2001), upward flow of air due to compression (Rommelaere et al., 1997), gradual trapping of air into bubbles (Schwander et al., 1988) and bubble close-off fractionation for smaller molecules (Huber et al., 2006).

Numerical models of the firn processes are important for interpreting firn and ice core measurements. The rate of diffusion of trace gases through the firn is a key model parameter, but it is not well known so firn models require calibration of the depth profile of diffusivity for each site. It is possible to measure the diffusivity in small firn samples (Schwander et al., 1988), however Fabre et al. (2000) concluded that variations in porosity would need to be known continuously and precisely over a larger scale than a core sample, particularly around the bottom of the firn, to reflect the macro scale variations in diffusivity and therefore be useful in firn models. Although there have been significant advances recently in characterizing the 3-dimensional structure of firn (Freitag et al., 2002, 2004), it remains to be seen whether lateral heterogeneities will limit the applicability of measurements on a core for representing the diffusivity in situ in the firn. Therefore, the approach of tuning the effective one-dimensional diffusivity by trying to match modelled and observed concentration profiles in the firn for one or more tracers with known atmospheric history (reference tracers) currently remains the most common, as well as the most accurate, way to estimate firn diffusivity.

Constraining firn diffusivity

C. M. Trudinger et al.

[Title Page](#)[Abstract](#)[Introduction](#)[Conclusions](#)[References](#)[Tables](#)[Figures](#)[I◀](#)[▶I](#)[◀](#)[▶](#)[Back](#)[Close](#)[Full Screen / Esc](#)[Printer-friendly Version](#)[Interactive Discussion](#)

Most studies have calibrated firm diffusivity using one or a few tracers, either manually (e.g. Trudinger et al., 1997) or with some kind of automated calibration method (e.g. Rommelaere et al., 1997). Two recent studies used up to 10 tracers at once (Buizert et al., 2012; Witrant et al., 2011). In most cases a single diffusivity profile is estimated without an uncertainty range, although Rommelaere et al. (1997) and Fabre et al. (2000) estimated the uncertainty by perturbing the concentration observations, and Buizert et al. (2012) compared diffusivity determined by six different firm models using the same dataset and physical firm characteristics.

There are three main types of uncertainty in model predictions (e.g. Højberg and Refsgaard, 2005). The first is related to data uncertainties, including calibration data and input data; this is generally the easiest type of uncertainty to deal with. The second is uncertainty related to model parameters, including the fact that when a problem is under-determined there will usually be multiple solutions that give an adequate match to observations – this is sometimes called equifinality (Beven, 2006) or the null space in linear algebra. The problem of tuning firm diffusivity using concentration profiles is often thought of as under-determined (Rommelaere et al., 1997; Buizert et al., 2012). While it has generally been assumed that as more tracers with different types of atmospheric history are used to tune the diffusivity profile it will be constrained more tightly, to our knowledge this assumption has not been tested or quantified. The third type of uncertainty, which is by far the most difficult to quantify but could be the most important uncertainty, is to do with model error, including the choice of processes included in the model and their mathematical formulations. This type of uncertainty is about how well the model processes represent the real world, and in firm models would include the assumption of one-dimensional diffusivity, as well as processes occurring in the lock-in zone that have received recent interest with some firm models now including dispersive mixing in this region (Severinghaus et al., 2010; Buizert et al., 2012). All three types of uncertainty are potentially important for firm modelling, but they are generally not taken into account when firm models are used to reconstruct atmospheric records of other tracers. The importance of the uncertainties will depend on how the model is

Constraining firm diffusivity

C. M. Trudinger et al.

[Title Page](#)[Abstract](#)[Introduction](#)[Conclusions](#)[References](#)[Tables](#)[Figures](#)[◀](#)[▶](#)[◀](#)[▶](#)[Back](#)[Close](#)[Full Screen / Esc](#)[Printer-friendly Version](#)[Interactive Discussion](#)

calibrated and what it is being used for. Our focus here will be mainly on the first two types of uncertainty, but we will touch on the third type. In particular, we wish to challenge the idea of using a single calibrated firm model, and suggest the use of multiple parameter sets to represent these uncertainties, as has become popular in other fields such as hydrology.

Here we describe an updated version of the CSIRO firm model (Trudinger et al., 1997) and use it to explore how well different combinations of tracers constrain the diffusivity profile and other parameters related to mixing. We use a global search method to locate multiple solutions that match the observations, initially with synthetic observations then with real observations from a number of sites. Most of our calculations relate to the NEEM site in Greenland, but we also model Antarctic sites DE08-2, DSSW20K and South Pole. We investigate whether we can estimate relative diffusion coefficients as part of model calibration, and look at how well we can constrain dispersive mixing in the lock-in zone. We also provide a way to represent the uncertainty due to equifinality, to determine the consequences of equifinality for inferring atmospheric histories of other trace gases in the firm.

2 Methods

In this section, we will describe the updated CSIRO firm model, our method for estimating diffusivity, the real and synthetic observations and other model inputs used.

2.1 CSIRO firm model

The CSIRO firm model is based on the model described by Trudinger et al. (1997) and Trudinger et al. (2002), but has been substantially improved and rewritten into Fortran90. Major changes from the previous version are (i) the inclusion of the upward flux of air due to compression of pore space that we had previously neglected, (ii) improved mass conservation of air in bubble trapping, (iii) a calibration routine using the genetic

Constraining firm diffusivity

C. M. Trudinger et al.

Title Page

Abstract

Introduction

Conclusions

References

Tables

Figures

◀

▶

◀

▶

Back

Close

Full Screen / Esc

Printer-friendly Version

Interactive Discussion



**Constraining firm
diffusivity**

C. M. Trudinger et al.

Title Page

Abstract

Introduction

Conclusions

References

Tables

Figures

◀

▶

◀

▶

Back

Close

Full Screen / Esc

Printer-friendly Version

Interactive Discussion



algorithm (GA) has been added to calibrate diffusivity and other parameters, (iv) an implicit time stepping scheme as in Rommelaere et al. (1997) has replaced the Euler predictor-corrector scheme (making a larger time step possible), (v) flux smoothing that was used by Trudinger et al. (1997) to keep the model stable is no longer required, (vi) an exponentially-decreasing eddy diffusion following Severinghaus et al. (2001) has been added as an alternative to a well-mixed layer to model convective mixing near the surface, and (vii) the option to include dispersive mixing in the lock-in zone following Severinghaus et al. (2010) and Buizert et al. (2012).

Like the old version of the CSIRO firm model, the new version uses a reference frame that moves downwards (relative to the surface) with the ice. In the Supplement, we describe derivation of the firm model equations in the moving reference frame. While the derivation of the equations in the moving coordinates may seem complicated because we take care to distinguish between quantities and derivatives in fixed and moving coordinates, the final equations that are solved in the moving coordinate system are no more complicated than those in the fixed reference frame.

The main advantage of using moving coordinates is that advection in open firm and trapped bubbles is treated in a consistent way over all depths. This makes it easy to model any overlap of the bubble trapping with diffusive mixing (which can cause additional age spread of trapped air compared to firm air), as well as any variations in the ice properties that move with the ice, such as a melt layer (Trudinger et al., 1997), or seasonal variations in ice properties (Trudinger, 2000).

The version of the CSIRO model that participated in the NEEM firm model intercomparison (Buizert et al., 2012) did not include the upward flux of air due to compression. Tests with and without this flux show that the fit to observations at NEEM can be substantially improved by including it. All results in the present paper include this flux.

Forward integration of the model equations requires specification of

- The atmospheric concentration history, $c_X(t)$, (used as a boundary condition).
- Site information: temperature, T , atmospheric pressure, P , accumulation rate, A .

- Density profile, $\rho(z)$ (from which other quantities such as total porosity $s(z)$ and vertical ice velocity $v(z)$ can be derived (note that $v(z)$ also depends on A)).
- Open porosity profile, $f(z)$ (we usually specify closed porosity $b(z)$ then $f(z) = s(z) - b(z)$).
- Diffusivity profile of CO_2 , $D_{\text{CO}_2}(z)$.
- Diffusion coefficient of tracer X relative to the diffusion coefficient of CO_2 : $\gamma_X \equiv D_X/D_{\text{CO}_2}$. Multiplying this by the diffusivity profile of CO_2 gives the diffusivity profile of tracer X , $D_X(z)$.
- Profile of eddy diffusion, $D_{\text{eddy}}(z)$ (the same for all tracers, used for convective mixing near the surface or dispersive mixing in the lock-in zone).
- Information about any other processes affecting mixing at a site, such as the depth of a well-mixed layer (representing convective mixing near the surface) or the date of creation and reduction of mixing of a melt layer.

The analysis in this paper involves solving the inverse problem of deducing $D_{\text{CO}_2}(z)$ from observations of multiple tracers. For some sites we also estimate parameters describing convective mixing or a melt layer. Additional cases involve the estimation of γ_X or dispersion in the lock-in zone. While we refer to the calibration observations as concentrations throughout the paper, they are actually mole fraction in dry air for most tracers, and isotopic ratios for the others.

2.2 Method for estimating diffusivity

We wish to estimate the depth profile of CO_2 diffusivity that minimizes the mismatch between modelled and observed concentration profiles. We specify diffusivity as a function of open porosity, as this relationship is more likely to be similar for different sites than diffusivity as a function of either density or depth. We assume that diffusivity decreases monotonically with depth to zero at the bottom of the firn, but otherwise wish

Constraining firn diffusivity

C. M. Trudinger et al.

Title Page

Abstract

Introduction

Conclusions

References

Tables

Figures

◀

▶

◀

▶

Back

Close

Full Screen / Esc

Printer-friendly Version

Interactive Discussion



Constraining firm diffusivity

C. M. Trudinger et al.

Title Page

Abstract

Introduction

Conclusions

References

Tables

Figures

◀

▶

◀

▶

Back

Close

Full Screen / Esc

Printer-friendly Version

Interactive Discussion



to avoid being prescriptive about the form of the function. For this reason we have chosen to define the diffusivity versus open porosity profile by interpolating with monotonic cubic splines (Wolberg and Alf, 2002) between about a dozen discrete points. The points are defined by fixing a diffusivity value and tuning the corresponding open porosity at which that diffusivity occurs (see Fig. 1). The exception is surface diffusivity, where we estimate the diffusivity corresponding to surface open porosity. The reason for tuning open porosity for fixed diffusivity, instead of tuning diffusivity for fixed open porosity, is to allow increased resolution as the diffusivity approaches zero (we do not know a priori for what values of open porosity the diffusivity will approach zero). Figure 1 shows the prior range for the open porosity values, f_n , corresponding to diffusivity $D_n = [0.0, 0.03, 0.05, 0.07, 0.1, 0.2, 0.5, 3.0, 20.0, 50.0, 110.0, 200.0, 300.0, 400.0]$ $\text{m}^2 \text{yr}^{-1}$ and the surface diffusivity value. This range is used for the initial calculations at NEEM, and a reduced range is used for later calculations. We use a genetic algorithm (Haupt and Haupt, 1998) to search for points that give the best agreement between modelled and measured firm concentrations of the reference tracers, by minimising the weighted root mean square mismatch, Φ , defined as

$$\Phi = \left(\frac{1}{N} \sum_{i=1}^N \frac{(m_i - d_i)^2}{\sigma_i^2} \right)^{\frac{1}{2}} \quad (1)$$

where N is the number of firm data, m_i and d_i are the modelled and measured firm concentrations, respectively, and σ_i are the one standard deviation uncertainties of the firm data (augmented to include other uncertainties as discussed in the next section).

Because we are only interested in monotonic solutions, and the interpolation by monotonic cubic splines will only work if the points are monotonic, any cases that the GA generates with points that are not monotonic (such as the case shown by the open triangles in Fig. 1) are not tested in the firm model, but instead assigned a cost function

value of Φ_{NM} defined as

$$\Phi_{\text{NM}} = 10^6 \times \sum_n |f_{n+1} - f_n| \quad (2)$$

where NM stands for non-monotonic and f_n is the open porosity value at point n . Values of Φ_{NM} are significantly larger than Φ from the firm model, and increase as the points depart further from monotonic. When fitting the monotonic spline (and also when checking for monotonicity of points), we ignore any points with diffusivity greater than the current surface value (e.g. in the case shown in Fig. 1 by the circles, the point at diffusivity = $400 \text{ m}^2 \text{ yr}^{-1}$ would be ignored). The prior ranges were chosen by trial and error to be large enough to include any solution that gives a good fit to the data.

For the GA calculation, we start with an ensemble of 500 randomly selected parameter sets and run the calculation for 30 000 generations, with the GA breeding and mutating parameter sets in the ensemble to obtain a new ensemble for each subsequent generation. Typically less than 10% (and sometimes as low as 1%, depending on the number of parameters being tuned and the ranges chosen) of the $500 \times 30\,000$ parameter sets tested will require a run of the firm model, the rest have non-monotonic points and therefore use Φ_{NM} . A typical calibration run takes 2–7 days to run on a PC.

In addition to estimating the parameters that define the CO_2 diffusivity profile, we include other parameters in the GA as required for each site, such as either the depth of a well-mixed layer, parameters defining an exponentially decreasing eddy diffusion for convective mixing near the surface, or the reduction of diffusivity associated with a melt layer that moves with the ice (see Supplement). We also include some calibrations fitting relative diffusion coefficients, γ_X . In the Supplement, we describe some calculations estimating four parameters in a simple function for dispersion in the lock-in zone.

To capture the range due to equifinality, as the GA runs we save the parameters and calculated depth profiles for any solution with Φ less than a chosen threshold. For most of the NEEM calculations described here we consider solutions with Φ up to 25%

Constraining firm diffusivity

C. M. Trudinger et al.

Title Page

Abstract

Introduction

Conclusions

References

Tables

Figures

◀

▶

◀

▶

Back

Close

Full Screen / Esc

Printer-friendly Version

Interactive Discussion



above the best solution. This range typically captures several thousand solutions that are all a good fit to the observations. For NEEM observations, our lowest value of Φ is 0.74, and 25 % above this gives 0.93 which is approximately the range covered by the models in Buizert et al. (2012). When selecting a threshold, we need to keep in mind the fact that our model is not a perfect representation of the real firm processes, and the data inevitably contain errors, so we should avoid retaining only the very best solutions.

To look at how well different combinations of tracers constrain diffusivity we will tune diffusivity using subsets of the available tracers for a site (with the set of all tracers being one of the subsets). We determine the threshold for Φ using all tracers and then use the same level for the other subsets (i.e. for NEEM we would use 0.93 for all subsets of tracers, even though some subsets have a best value of Φ below 0.74). We will refer to solutions that have Φ below the threshold as the accepted solutions.

We can relate our choice of threshold for Φ to a confidence interval using the F ratio test (Árnadóttir and Segall, 1994; Seber and Wild, 2005). The value of Φ that corresponds to a $100 \times (1 - \alpha)\%$ confidence level is determined from

$$\Phi^2 = \Phi_{\text{opt}}^2 \left[1 + \frac{p}{n-p} F(p, n-p, 1-\alpha) \right] \quad (3)$$

where Φ_{opt} is the optimal value of Φ , p is the number of parameters estimated, n is the number of observations and $F(p, n-p, 1-\alpha)$ is the F distribution with p and $n-p$ degrees of freedom at a $100 \times (1 - \alpha)\%$ confidence level (Draper and Smith, 1981). Therefore all models with Φ less than this threshold are consistent with the optimal model at the specified confidence level. Note that these confidence intervals are only approximate, as they assume Gaussian errors and linear variation of Φ around the minimum. They are also subject to our assumption of monotonic diffusivity profiles, and to our choice of processes to represent which determines the number of parameters we estimate.

By applying the same threshold to different subsets (each with different numbers of observations), our results for each subset correspond to different confidence levels

Constraining firm diffusivity

C. M. Trudinger et al.

Title Page

Abstract

Introduction

Conclusions

References

Tables

Figures

◀

▶

◀

▶

Back

Close

Full Screen / Esc

Printer-friendly Version

Interactive Discussion



(e.g. for 16 parameters and 220 observations, the threshold of 1.25 times Φ_{opt} corresponds to a confidence level of almost 100 %, but the same threshold with only 44 observations would correspond to a confidence level of 50 %). However, we choose to use a fixed threshold so that we can compare the results of calibrations that fit the observations to the same degree. The alternative of changing the threshold for different subsets to correspond to the same confidence level is equally valid, but in that case a significant amount of the difference in spread between subsets will be due to the different number of observations, which is not what we are interested in at present.

It should be noted that our method is not very efficient at finding the one diffusivity profile that gives the best fit to the observations. Down-gradient search methods are more suited for that purpose. The GA, on the other hand, is well suited to locating a large range of diffusivity profiles and other parameters that fit the observed concentrations up to a certain threshold.

2.3 Observations and model inputs

2.3.1 NEEM

Most of our calculations relate to the NEEM 2008 firn air campaign (Buizert et al., 2012). From that study we use firn air data for 10 tracers from the S2 borehole at NEEM, Greenland (CO_2 , CH_4 , SF_6 , CFC-11, CFC-12, CFC-113, CH_3CCl_3 (methyl chloroform), HFC-134a, $^{14}\text{CO}_2$ and $\delta^{15}\text{N}_2$), uncertainty estimates (based on a range of contributions including analytical precision and uncertainty in atmospheric histories), and the physical firn characteristics (see Table 1). The fit to the reference tracers as calculated with Eq. (1) using the NEEM observations and uncertainties from Buizert et al. (2012) is denoted Φ_{N} .

The concentration histories for the gases considered in this paper are described and shown in the Supplement. We use the relative diffusion coefficients from Matsunaga et al. (1993, 1998, 2002). For all of the sites we consider, we follow Buizert et al.

Constraining firn diffusivity

C. M. Trudinger et al.

Title Page

Abstract

Introduction

Conclusions

References

Tables

Figures

◀

▶

◀

▶

Back

Close

Full Screen / Esc

Printer-friendly Version

Interactive Discussion



(2012) by converting firn measurements and atmospheric histories of $\Delta^{14}\text{CO}_2$ in ‰ to $^{14}\text{CO}_2$ in ppm, as well as modelling $\delta^{15}\text{N}_2$ using a single $^{15}\text{N}^{14}\text{N}$ tracer.

2.3.2 NEEM synthetic observations

In order to test our method for estimating diffusivity, and to see how well different tracers constrain diffusivity in an ideal situation without the complications of real observations and an imperfect model, we generate two synthetic data sets for NEEM, for use in addition to the real observations from the NEEM intercomparison.

“Synthetic A” has 22 observations for each of the 10 tracers, at depths matching the NEEM observation depths excluding the surface. We generated the true concentrations by running our firn model with the molecular diffusivity tuned to S2 NEEM observations in Buizert et al. (2012) with the LGGE-GIPSA firn model, and a 3.66 m well-mixed layer. We added uncorrelated random noise to each synthetic observation. We shifted and scaled the random noise so that the mean of the noise added to each tracer was zero and the standard deviation was exactly 0.5 % of the range of each tracer (maximum minus minimum values of the synthetic observations). The comparison of modelled concentration profiles with the Synthetic A observations using Synthetic A uncertainties is denoted Φ_A . The data uncertainty σ_i used in Φ_A matches the standard deviation of the noise added to each tracer.

“Synthetic B” has the same true concentration as Synthetic A, but observations correspond exactly to the types and measurement depths for the EU borehole in the NEEM intercomparison (between 15 and 23 measurements of each tracer). Three types of error are added to the synthetic observations: (1) random error with zero mean and $\text{sd} = 0.5\%$ of the range, (2) systematic offset added to each tracer, where the magnitude of the offset (a constant value for each tracer) is a random number with $\text{sd} = 1\%$ of the range for each tracer, and (3) systematic error that increases linearly with depth from zero at the surface to a value at 80 m that is a random number with $\text{sd} = 2\%$ of the range for each tracer. The comparison of modelled concentration

Constraining firn diffusivity

C. M. Trudinger et al.

Title Page

Abstract

Introduction

Conclusions

References

Tables

Figures

◀

▶

◀

▶

Back

Close

Full Screen / Esc

Printer-friendly Version

Interactive Discussion



profiles with the Synthetic B observations using Synthetic B uncertainties is denoted Φ_B . Depending on the random values generated, some tracers will have larger systematic errors added than others. The data uncertainty used to calculate Φ_B is $\sigma_i = R \times \sqrt{(0.005^2 + 0.01^2 + (0.02 \cdot z_i / 80)^2)}$ where R is the range for each tracer described above. This case is more like reality, where systematic errors probably dominate, than Synthetic A. The uncertainties on the NEEM observations from Buizert et al. (2012) were often around 1–2 % of the range for each tracer, with some larger values for various reasons, so this case is similar to the real NEEM case.

2.3.3 Subsets of NEEM tracers

For the NEEM calculations (with both synthetic and real observations) we look at the diffusivity estimated with observations of all ten tracers, as well as other subsets of tracers as listed in Table 2. The subsets were chosen by starting with a minimum set that might be used, CH_4 and $\delta^{15}\text{N}_2$; these are two tracers that have been measured at almost all (if not all) firn air sites. We then add one tracer at a time with the aim that each new tracer will add new information to improve the constraint on diffusivity. This is based on the expectation that tracers with atmospheric records covering different periods will constrain diffusivity in different parts of the profile. CO_2 and $^{14}\text{CO}_2$ were excluded from the subsets because of concerns of possible contamination in Northern Hemisphere firn, even though this is not an issue with synthetic data. For Synthetic A, we also compare results using each of the ten tracers separately.

In comparing these subsets, we will compare both the best case for each subset as well as the range of accepted solutions.

2.4 DE08-2

DE08-2 is located on the east side of Law Dome, East Antarctica (Etheridge et al., 1996, 1998; Trudinger et al., 1997) and firn air was sampled in 1993. Site parameters are given in Table 1. For density versus depth we use a spline fit to measurements from

Constraining firn diffusivity

C. M. Trudinger et al.

Title Page

Abstract

Introduction

Conclusions

References

Tables

Figures

◀

▶

◀

▶

Back

Close

Full Screen / Esc

Printer-friendly Version

Interactive Discussion



Etheridge and Wookey (1989) and Etheridge et al. (1996). For closed porosity versus density we use a spline fit to measurements by J.-M. Barnola (unpublished data) with a cut bubble correction (J.-M. Barnola, personal communication, 1999) which gives a rapid reduction of open porosity to zero around 90 m, in line with the observation that there was still good flow of firn air at 85 m, but no air could be pumped from the firn at 90 m (Etheridge et al., 1996).

The ice structure at DE08-2 shows a melt layer at 8.7 m below the surface. Trudinger et al. (1997) found that the agreement between modelled and measured tracers at DE08-2 (SF_6 in particular) was significantly improved by including a melt layer that originated at the surface in the 1989–1990 summer and moved with the ice with a reduction in the diffusive flux of about 80 %. Here we model the melt layer as originating at the surface in 1989.77 and moving with the ice as described in the Supplement. We tune the reduction in mixing along with the diffusivity profile using measurements of CO_2 , CH_4 , SF_6 , $\delta^{15}\text{N}_2$ and $^{14}\text{CO}_2$ (Etheridge et al., 1996; Trudinger et al., 1997; Levchenko et al., 1997). DE08-2 firn measurements and the uncertainties we use are given in the Supplement.

2.5 DSSW20K

DSSW20K is located on the lower-accumulation-rate west side of Law Dome, East Antarctica and firn air was sampled in January 1998 (Smith et al., 2000; Sturrock et al., 2002; Trudinger et al., 2002). The firn column at DSSW20K is relatively short, with a lock-in depth of about 43 m. We use a spline fit to DSSW20K density measurements, and the DE08-2 closed porosity spline. DSSW20K has a region of convective mixing near the surface that was modelled by Trudinger et al. (2002) using a 4 m well-mixed region. Here we use either an exponentially-decreasing eddy diffusion or well-mixed layer and tune the relevant parameters along with the diffusivity profile with measurements of CO_2 , CH_4 , SF_6 , $\delta^{15}\text{N}_2$, $^{14}\text{CO}_2$, HFC-134a, HCFC-141b, CFC-11, CFC-12, CFC-113 and CH_3CCl_3 (Smith et al., 2000; Sturrock et al., 2002; Trudinger et al., 2002). The

Constraining firn diffusivity

C. M. Trudinger et al.

Title Page

Abstract

Introduction

Conclusions

References

Tables

Figures

◀

▶

◀

▶

Back

Close

Full Screen / Esc

Printer-friendly Version

Interactive Discussion



DSSW20K firn measurements and the uncertainties we use are given in the Supplement.

Southern Hemisphere atmospheric histories of SF₆, CH₃CCl₃ and the CFCs prior to 1978 (when the Cape Grim Air Archive and/or Cape Grim in situ measurements began) are based on emissions estimates rather than atmospheric measurements (see Supplement). For DSSW20K, we choose not to use concentration measurements of these tracers below 45 m in our model calibration because of the greater uncertainty in their atmospheric histories. The alternative approach is to include the firn observations with larger uncertainties to reflect the greater uncertainty in the atmospheric histories – this is the approach we have used for NEEM, because we use exactly the same dataset as Buizert et al. (2012) to allow direct comparison, and this is their approach. Although we have not done it here, it would be easy to test the sensitivity of calibration results to including or excluding these observations.

2.6 South Pole

Firn air was collected from South Pole, Antarctica in 1995 (Battle et al., 1996; Butler et al., 1999) and again in 2001 (Butler et al., 2001; Aydin et al., 2004; Sowers et al., 2005). Following previous work for South Pole, we treat these as two separate sites. We use the site properties in Table 1, a spline fit to South Pole density measurements (different for 1995 and 2001 drillings) from Mark Battle (personal communication, 2012) and the DE08-2 closed porosity spline. For South Pole 1995 we use measurements of CO₂, CH₄, SF₆, δ¹⁵N₂, CFC-11, CFC-12 and CH₃CCl₃ (Battle et al., 1996; Butler et al., 1999). For South Pole 2001 we use CO₂, CH₄, SF₆ and δ¹⁵N₂ (Aydin et al. (2004); Sowers et al. (2005); Witrant et al. (2011); M. Battle, personal communication, 2012). For both South Pole sites we omit firn concentration measurements corresponding to ages before 1978 for tracers with atmospheric histories based on emissions estimates.

Constraining firn diffusivity

C. M. Trudinger et al.

Title Page

Abstract

Introduction

Conclusions

References

Tables

Figures

◀

▶

◀

▶

Back

Close

Full Screen / Esc

Printer-friendly Version

Interactive Discussion



2.7 Relative diffusion coefficients

As well as there being uncertainty in the CO₂ diffusivity profile, there is also uncertainty in the relative diffusion coefficients, $\gamma_X = D_X/D_{\text{CO}_2}$. Previous firm studies have used quite a wide range of relative diffusion coefficients. For example, some values of γ_{CH_4} that have been used in past firm modelling studies include 1.35 for Summit (Schwander et al., 1993), 1.29 for DE08-2 (Trudinger et al., 1997), 1.415 for DE08-2 (Rommelaere et al., 1997; Martinerie et al., 2009) and the value used here of 1.367 (Buizert et al., 2012). For γ_{SF_6} there has been 0.582 (Trudinger et al., 1997), 0.621 (Martinerie et al., 2009) and 0.554 used here from Buizert et al. (2012). This variation corresponds to roughly $\pm 5\%$ variation around the middle of the range; less than 1% of this variation can be ascribed to differences in temperature. The different estimates of γ_X were based on measurements, data compilations and empirical equations from various sources (Andrussow et al., 1969; Marrero and Mason, 1972; Fuller et al., 1966; Chen and Othmer, 1962; Lugg, 1968). The values of γ_X used in Buizert et al. (2012) were based on a consistent set of diffusivity measurements from Matsunaga et al. (1993, 1998, 2002) with estimated uncertainty of about $\pm 2\%$.

Due to the different estimates available for relative diffusion coefficients, Trudinger et al. (2002) tuned γ_{SF_6} and $\gamma_{\text{HFC}_{134a}}$ at DSSW20K, obtaining values 0.628 and 0.614, respectively. Trudinger (2000) found best agreement to South Pole CH₄ with γ_{CH_4} of 1.42. Butler et al. (1999) also adjusted $\gamma_{\text{CFC}_{11}}$ by 10% to fit observations better. In Sect. 3.8 we will investigate tuning the relative diffusion coefficients with the GA using both the pseudo and real observations.

2.8 Dispersion in the lock-in zone

Dispersion has recently been included in a number of firm models to improve the fit to observations (Severinghaus et al., 2010; Buizert et al., 2012). The dispersive mixing term is mathematically identical to the eddy diffusion term, with a transport flux that is equal for all tracers and their isotopologues. Dispersion therefore gives no gravitational

Constraining firm diffusivity

C. M. Trudinger et al.

[Title Page](#)[Abstract](#)[Introduction](#)[Conclusions](#)[References](#)[Tables](#)[Figures](#)[◀](#)[▶](#)[◀](#)[▶](#)[Back](#)[Close](#)[Full Screen / Esc](#)[Printer-friendly Version](#)[Interactive Discussion](#)

separation with depth, consistent with observations of $\delta^{15}\text{N}_2$ in the lock-in zone. Severinghaus et al. (2010) and Buizert et al. (2012) discuss the physical reasons to believe some dispersive mixing occurs in the lock-in zone. In Buizert et al. (2012) the different treatment of mixing in the lock-in zone (some firm models used dispersion, others molecular diffusion) was believed to have caused significant variation in diffusive fractionation of isotopes (Trudinger et al., 1997). As firm models are often used to infer atmospheric histories of isotopes, improvement of our understanding of lock-in zone processes and proper characterisation of the uncertainties are important. In the Supplement, and summarised in Sect. 3.9, we look at the sensitivity of concentration profiles to dispersion, and add dispersion to some model calibrations. These calculations are a start to accounting for model error in our uncertainty estimates.

3 Results

3.1 NEEM Synthetic A

3.1.1 Comparison of subsets

We first consider the case with synthetic observations for NEEM and only uncorrelated random noise (Synthetic A). Figure 2 shows the concentration profiles for Synthetic A using only observations of CH_4 and $\delta^{15}\text{N}_2$ for calibration (Subset Two, in panels a–j), and using all ten tracers for calibration (Subset Ten, in panels k–t). Figure 3 shows the diffusivity profiles and CH_3CCl_3 for all five Subsets in Table 2. We show the true solution (red solid lines), best case (solid black lines), upper and lower values of the range of accepted solutions ($\Phi_A < 1.25$, dotted black lines) and 19 representative solutions (blue lines) selected from the set of all accepted solutions. If all of the accepted solutions were plotted, the region between the black dotted lines would be almost completely shaded. The representative solutions cover different values of Φ_A over the range between the lowest value (0.86 for Two and 1.03 for Ten) and 1.25, and include solutions

Constraining firm diffusivity

C. M. Trudinger et al.

[Title Page](#)[Abstract](#)[Introduction](#)[Conclusions](#)[References](#)[Tables](#)[Figures](#)[◀](#)[▶](#)[◀](#)[▶](#)[Back](#)[Close](#)[Full Screen / Esc](#)[Printer-friendly Version](#)[Interactive Discussion](#)

that differ most from the best solution and each other. Representative solutions such as these will be used to represent equifinality in the firn model when it is used to infer atmospheric histories of other trace gases.

Table 3 gives the weighted RMS mismatch of each best solution from the noisy synthetic observations for each tracer separately and together for the five Subsets considered, with numbers shown in bold if that tracer was used for calibration in that experiment. Table 3 also gives the weighted RMS mismatch of each best solution from the true concentrations weighted by the same data uncertainties, denoted Φ_{At} .

The diffusivity profile was not well constrained with CH_4 and $\delta^{15}\text{N}_2$ alone. CH_4 does not vary much with depth above 65 m, so there is not much information to distinguish between diffusion in different parts of the firn above 65 m. While $\delta^{15}\text{N}_2$ is quite sensitive to the depth of the well-mixed layer, it is fairly insensitive to the diffusivity profile within the parameter range considered. In contrast, diffusion around 65–70 m is quite tightly constrained (small spread of solutions). Calibrating with only these two tracers, the best estimate of diffusivity and the best concentration profiles of most tracers not used in the GA are quite different from the true profiles ($\Phi_{At} = 4.57$). There is also significant spread in solutions with $\Phi_A < 1.25$, with spread being greatest for CH_3CCl_3 that has a rapid recent atmospheric decrease, followed by HFC-134a that has a rapid recent rise in the atmosphere. Apart from the two tracers used for calibration, $^{14}\text{CO}_2$ has the next smallest spread above the lock-in depth. With little variation with depth above 65 m, this part of the $^{14}\text{CO}_2$ profile would provide little additional information if used for calibration. However, the peak in $^{14}\text{CO}_2$ at NEEM is below the lock-in depth, and there is some spread in solutions around the peak and even more spread around 75–80 m, suggesting that it could be a useful tracer in this region, particularly as the other tracers have either zero concentrations or very little spread there.

When all ten tracers were used for calibration, the diffusivity and concentration profiles for the best solution were close to the true profiles ($\Phi_{At} = 0.44$) and the weighted RMS mismatch from the noisy observations was around 1.0 (HFC-134a and CFC-12 had the highest mismatch and $^{14}\text{CO}_2$ the lowest). The spread in concentrations of

Constraining firn diffusivity

C. M. Trudinger et al.

Title Page

Abstract

Introduction

Conclusions

References

Tables

Figures

◀

▶

◀

▶

Back

Close

Full Screen / Esc

Printer-friendly Version

Interactive Discussion



these ten tracers for solutions with Φ_A up to 1.25 was very small; the only tracers for which the difference between the maximum and minimum curves is big enough to be seen in panels k–t of Fig. 2 are CH_3CCl_3 and HFC-134a, and to a lesser extent SF_6 , as the fit to these tracers varies most within the range of solutions with $\Phi_A < 1.25$.

There is a clear difference between Subset Two and the other four in Fig. 3. Adding just SF_6 to the calibration (Subset Three) makes a large difference in reducing the spread of accepted solutions, and in bringing the best solution closer to the true profile. There is further improvement to the best solution by adding HFC-134a (Subset Four), but little further improvement beyond this up to the ten tracers other than some reduction in spread below 70 m from Subset Five to Ten. Of the five sets of observations considered, Subset Four has estimated diffusivity closest to the true diffusivity. It is encouraging that in this simplest case with uncorrelated errors, we can reconstruct diffusivity well with four or more tracers and our specification of diffusivity using cubic splines between a small number of points.

The Synthetic A observations have been set up so that the true diffusivity corresponds to Φ_A of exactly 1.0 for all tracers separately and together (see Table 3). Values of Φ_A for the best solutions of the different Subsets (for observations actually fitted) vary from 0.86 to 1.03, generally lower than 1.0 for two to four tracers and around 1.0 for five and ten tracers. The lower values of Φ_A are achieved by fitting to some of the noise, i.e. overfitting the noisy data. Diffusion in the firn leads to smooth profiles of concentration with depth, so we did not expect that there would be much overfitting of the Synthetic A observations that have only uncorrelated noise, but the GA does manage to find solutions that are closer to the observations, quantified by the RMS difference, than the true solution. Overfitting decreases as more tracers are added, and by five tracers we have essentially stopped overfitting the noisy data.

The depth of the well-mixed layer was estimated as part of the inversion, and when $\delta^{15}\text{N}_2$ was used for calibration the depth for the solution with lowest Φ_A was always close to the true value of 3.66 with a clear increase in Φ_A moving away from this value.

Constraining firn diffusivity

C. M. Trudinger et al.

[Title Page](#)[Abstract](#)[Introduction](#)[Conclusions](#)[References](#)[Tables](#)[Figures](#)[I◀](#)[▶I](#)[◀](#)[▶](#)[Back](#)[Close](#)[Full Screen / Esc](#)[Printer-friendly Version](#)[Interactive Discussion](#)

In a calibration calculation without $\delta^{15}\text{N}_2$ but with the other nine tracers, the well-mixed layer was not quite as well resolved.

3.1.2 Single tracer calibrations

We also tested calibration of diffusivity and the well-mixed layer depth with each of the ten tracers taken separately. Figure 4 shows the range (i.e. maximum minus minimum) of accepted concentration profiles ($\Phi_A < 1.25$) for all ten tracers when only one tracer was used for calibration (i.e. this corresponds to the difference between the black dotted lines in earlier plots). On its own, $\delta^{15}\text{N}_2$ has the weakest constraint on diffusivity and therefore leads to the largest spread in the other nine tracers. Constraining diffusivity with either CH_4 or $^{14}\text{CO}_2$ gave the next largest spread in the other tracers above 60 m, but leads to lower spread below this, and in fact calibrating with just $^{14}\text{CO}_2$ gave the smallest spread for all tracers below 70 m. Next best at constraining diffusivity are CFC-11, CFC-12 and CFC-113, in that order; having little variation with depth they do not provide a strong constraint for the tracers with rapid atmospheric growth rates. SF_6 and CO_2 provide the next best constraints above 60 m, and CO_2 is one of the best tracers below 60 m. HFC-134a provided a very good constraint on other tracers through most of the firn (to around 62 m), but the weakest constraint below this where concentrations are small. CH_3CCl_3 provided the strongest constraint on the other tracers above 60 m.

When we calibrate the model with only one tracer, the closest fit to the noisy observations of all ten tracers, and to the truth for all ten tracers, is achieved by calibrating with CH_3CCl_3 ($\Phi_A = 1.59$ and $\Phi_{A_t} = 1.32$), where a significant fraction of the mismatch comes from $^{14}\text{CO}_2$ with some also from CO_2 and CH_4 in the lock-in zone, as well as $\delta^{15}\text{N}_2$. CFC-113 comes a close second overall ($\Phi_A = 1.66$ and $\Phi_{A_t} = 1.35$), with the misfit to $\delta^{15}\text{N}_2$ and $^{14}\text{CO}_2$ being the highest contributors to the mismatch. The next best tracers on their own are SF_6 , CO_2 , CFC-12 and HFC-134a, with Φ_A for all tracers in the range 2–2.5 and significant contributions to their overall misfits from one or a few of CH_3CCl_3 , $^{14}\text{CO}_2$ and $\delta^{15}\text{N}_2$. The worst tracers on their own are CH_4 , CFC-11,

Constraining firn diffusivity

C. M. Trudinger et al.

Title Page

Abstract

Introduction

Conclusions

References

Tables

Figures

◀

▶

◀

▶

Back

Close

Full Screen / Esc

Printer-friendly Version

Interactive Discussion



$\delta^{15}\text{N}_2$ and $^{14}\text{CO}_2$, with Φ_A and also Φ_{At} in the range 4.5–6.5 with very large contributions to their overall misfits from CH_3CCl_3 and HFC-134a followed by SF_6 . Conclusions from these two ways of looking at the results (spread and best solutions) are similar: CH_3CCl_3 , HFC-134a, SF_6 and CO_2 stand out as important above the lock-in depth, and tracers that have been in the atmosphere longer like CH_4 , CO_2 and especially $^{14}\text{CO}_2$ with its variation due to the bomb pulse are important in the lock-in zone.

3.1.3 Synthetic A age distributions

The diffusivity profile is a model-dependent quantity and of secondary importance compared to the age distribution which characterizes the firn air transport characteristics and is more useful for comparison between firn models and use in inversions for atmospheric histories (Rommelaere et al., 1997; Trudinger et al., 2002). Figure 5 shows CO_2 age distributions in firn air at 63 m (the lock-in depth) and 78 m at NEEM for the five Subsets of Synthetic A observations in Table 2 plus the case calibrating to CH_3CCl_3 alone, and a case with $\delta^{15}\text{N}_2$, CH_3CCl_3 and $^{14}\text{CO}_2$ (see below).

We can quantify the width of the age distribution with the spectral width, Δ , defined as

$$\Delta^2(z) = \frac{1}{2} \int_0^{\infty} (t - \Gamma)^2 G(z, t) dt \quad (4)$$

where t is time, z is depth and Γ is the mean of the age distribution, G (Trudinger et al., 2002). On the right side of Fig. 5 we show variation of Δ with depth for the same seven subsets, as well as the range in spectral width for the ensemble of 20 representative solutions in each case (Fig. 5o). This figure shows the large reduction in spread in the calculated age distributions above 60 m going from Subset Two to Three, then the slight improvement from Subset Three to Four but little reduction beyond this for most of the firn. Between 10 m and 65 m, CH_3CCl_3 has done as well as all ten tracers in

Constraining firn diffusivity

C. M. Trudinger et al.

Title Page

Abstract

Introduction

Conclusions

References

Tables

Figures

◀

▶

◀

▶

Back

Close

Full Screen / Esc

Printer-friendly Version

Interactive Discussion



constraining the age distribution with the Synthetic A observations, but below 65 m the spread is large and it is the worst of these cases below 70 m. Below 70 m, Subset Ten is significantly better than all other Subsets, presumably because it is the only one that includes $^{14}\text{CO}_2$. Both Subset Two and CH_3CCl_3 have larger spread at 5 m than the other cases. Adding just SF_6 reduces the spread at 5 m to be similar to the other cases. This implies that to constrain the model near the surface we should use $\delta^{15}\text{N}_2$ and a tracer with a significant concentration gradient near the surface.

If we were to select the minimum number of tracers to constrain diffusivity with the Synthetic A observations, based on these calculations we would choose $\delta^{15}\text{N}_2$, CH_3CCl_3 and $^{14}\text{CO}_2$. The age distributions and spectral widths for this combination of tracers are shown in Fig. 5, and they have done a very good job at reducing the spread in solutions. The spread in solutions below 70 m is lower for these three tracers than for Subset Ten, presumably because they give a more equal weighting to tracers with information content above and below the lock-in zone, unlike Subset Ten which has many more tracers with information content above 70 m, so (with the same Φ threshold used for both cases) the GA can find solutions with Subset Ten that relax the fit to the couple of tracers with variation below 70 m and still have Φ_A below the threshold.

It is very important to remember that the Synthetic A data has small, Gaussian errors that are the same for all tracers relative to their overall range of variation in the firn. This tells us about the information content of the tracers largely without consideration of data errors that would be likely to be found in a realistic case.

3.2 NEEM Synthetic B

The second synthetic case has the same true diffusivity but more complicated data errors and different numbers of observations of each tracer. This is a more realistic case that probably resembles a true firn air site more closely than Synthetic A. Figure 6 shows the diffusivity profiles and CH_3CCl_3 determined by calibrating with these observations. With a lowest value of Φ_B of 0.8 for Subset Ten, we consider solutions

Constraining firn diffusivity

C. M. Trudinger et al.

[Title Page](#)[Abstract](#)[Introduction](#)[Conclusions](#)[References](#)[Tables](#)[Figures](#)[◀](#)[▶](#)[◀](#)[▶](#)[Back](#)[Close](#)[Full Screen / Esc](#)[Printer-friendly Version](#)[Interactive Discussion](#)

with Φ_B up to 1.0 for all Synthetic B subsets. Table 3 shows weighted RMS mismatch of the best solutions from the observations (Φ_B) and from the truth for Synthetic B experiments, where we have used the Synthetic A true observations and uncertainties to calculate the mismatch from the truth, to allow better comparison with the results from Synthetic A experiments (this is therefore denoted Φ_{At}).

Compared to Synthetic A, the results for Synthetic B are further from the true solution, and the spread in diffusivity for the range of accepted solutions is significantly greater (from comparing Figs. 3 and 6). None of the Subsets using Synthetic B observations is closer to the true solution than Subset Three with Synthetic A observations and uncertainties. This is not surprising, because of the larger and more complicated (non-Gaussian) errors in the Synthetic B observations. Despite the results being worse than for Synthetic A, we do manage to reconstruct the diffusivity profile reasonably well for four or more tracers. Perhaps coincidentally, Subset Four again has the closest match to the true observations of the five Subsets considered. Compared to Subset Five, Subset Ten has an improvement in the best solution in the deep firn as well as a reduction in the spread of accepted solutions in this region.

Figure 7a shows the range in the spectral width of the age distribution with depth for solutions with $\Phi_B < 1.0$ in the five Subsets. To show the sensitivity of this variation to a different choice of Φ_B threshold, Fig. 7b shows the same plot for $\Phi_B < 0.88$ which is 10% above the best solution for Synthetic B Subset Ten. The features are generally similar for these two choices of threshold. There is a reduction in all curves, but a larger relative reduction for Subset Ten in the lock-in zone. The variation in the best solution and spread of solutions for Synthetic B Subsets is quite similar to those for Synthetic A.

For Synthetic B, the true diffusivity gives Φ_B of 0.81, and the best cases have values of Φ_B for fitted observations between 0.62 and 0.8, with only Subset Ten having Φ_B near the true value of 0.81. In both Synthetic A and B, the model fits the data better than the true values for small numbers of tracers. Overfitting of the data is more of a problem for Synthetic B than A, as expected, with lower values of Φ relative to the Φ for the true solution and we needed five tracers to avoid it with Synthetic A but at

Constraining firn diffusivity

C. M. Trudinger et al.

Title Page

Abstract

Introduction

Conclusions

References

Tables

Figures

◀

▶

◀

▶

Back

Close

Full Screen / Esc

Printer-friendly Version

Interactive Discussion



least six and possibly up to ten tracers for Synthetic B (noting that we did not have Subsets with six to nine tracers). Even though in both synthetic datasets the best case in Subset Four had the closest solution to the truth, the values of Φ_A and Φ_B show that they are overfitting the data more than Subsets Five and Ten, presumably this is simply because it is harder to overfit the data as more tracers are used.

3.3 NEEM

We now look at the results using the real observations from the NEEM intercomparison by Buizert et al. (2012), with the same five subsets of tracers as used for the synthetic observations. Table 4 shows the weighted RMS mismatch from NEEM observations (Φ_N). All five Subsets used a well-mixed layer for convective mixing near the surface. We also tried Subset Ten with exponentially-decreasing eddy diffusion for convective mixing (Severinghaus et al., 2001) instead of the well-mixed layer (denoted TenEddy), and achieved Φ_N that was lower by only 0.01 than the well-mixed layer case. The diffusivity and concentration profiles for TenEddy are shown in Fig. 8, with solutions up to $\Phi_N = 0.93$ that corresponds to the range from Buizert et al. (2012) and a confidence level of almost 100 % (for the number of parameters we are estimating).

With a best value of $\Phi_N = 0.74$ for NEEM TenEddy, our results are now much better than the case with the CSIRO model shown in Buizert et al. (2012) that omitted the upward flux of air due to compression of firn channels and had $\Phi_N = 0.92$. Like the other models in Buizert et al. (2012), we have diffusion (in our case it is molecular) of around $0.1 \text{ m}^2 \text{ yr}^{-1}$ below the lock-in depth of around 63 m. Our modelled $\delta^{15}\text{N}_2$ increases very slightly through the lock-in zone, at a rate of about $0.0004 \text{ \%} \cdot \text{m}^{-1}$, which is as consistent with the observations as constant levels.

The depth of the well-mixed layer was estimated as part of the inversion, and was always well resolved with a clear minimum in Φ_N when $\delta^{15}\text{N}_2$ was used for calibration, but was not resolved at all within the prior range of 2 to 5 m in a calibration that included all tracers except $\delta^{15}\text{N}_2$.

Constraining firn diffusivity

C. M. Trudinger et al.

[Title Page](#)[Abstract](#)[Introduction](#)[Conclusions](#)[References](#)[Tables](#)[Figures](#)[◀](#)[▶](#)[◀](#)[▶](#)[Back](#)[Close](#)[Full Screen / Esc](#)[Printer-friendly Version](#)[Interactive Discussion](#)

Variation in the best values of Φ_N for the five Subsets with NEEM observations is somewhat similar to the Synthetic B variation, although NEEM has a bit larger relative change between Subsets in the fitted observations and a bit smaller relative change in the fit to all ten tracers.

While many of the uncertainties in the real NEEM observations are around 1–2% of the range of concentrations for each tracer, similar to the Synthetic B observations, there are some tracers and depth ranges that have larger uncertainties (e.g. $^{14}\text{CO}_2$ has uncertainties around 6%, CO_2 has uncertainties of 1–2% through most of the firn but around 3% in the upper region and around 8% in the lower firn and CH_3CCl_3 has uncertainties around 8% for the highest concentrations). This will change the relative constraints provided by the different tracers compared to the synthetic cases that have less variation in the uncertainties of different tracers.

Figure 7c shows the variation with depth in the spectral width range for the Subsets with NEEM observations. Compared to Subset Two, Subset Three constrains the spectral width much better above the lock-in depth, but worse below it. This is probably a consequence of using the same threshold for both Subsets, so that in Subset Three if it is possible to fit the SF_6 observations well within the uncertainties through the diffusive part of the firn this leaves scope to include solutions that are a worse fit to observations in the lock-in zone and still be in the range $\Phi_N < 0.93$ overall. The range in spectral widths for the NEEM observations is larger than for the Synthetic B observations due to the larger observation uncertainties, but the comparison between different Subsets is generally similar to Synthetic B.

We can get an indication of how useful additional tracers would be for constraining diffusivity at NEEM by running the model in a forward sense with our ensemble of representative diffusivity profiles to see how much the modelled concentration profiles vary. We tried this for CCl_4 (which increases in the atmosphere from about 1920 until 1990 followed by a decrease), HCFC-142b (gradually increases from the early 1970s followed by a much more rapid increase from around 1990) and HFC-43-10mee (rapid increase from 2002). Although we do not have firn measurements of these tracers,

Constraining firn diffusivity

C. M. Trudinger et al.

[Title Page](#)[Abstract](#)[Introduction](#)[Conclusions](#)[References](#)[Tables](#)[Figures](#)[◀](#)[▶](#)[◀](#)[▶](#)[Back](#)[Close](#)[Full Screen / Esc](#)[Printer-friendly Version](#)[Interactive Discussion](#)

Constraining firm diffusivity

C. M. Trudinger et al.

Title Page

Abstract

Introduction

Conclusions

References

Tables

Figures

◀

▶

◀

▶

Back

Close

Full Screen / Esc

Printer-friendly Version

Interactive Discussion



the spread in the calculated concentration depth profiles will suggest whether tracers such as these would be useful for calibration if they were measured in the firm and we knew their atmospheric histories accurately enough. Atmospheric histories and firm depth profiles calculated with diffusivity from NEEM case TenEddy are shown in Fig. 9.

5 The spread of concentration profiles is quite small for CCl_4 , suggesting that it would not add significant new information beyond what we already have from the ten tracers (apart from the degree to which additional observations with independent errors reduce the possibility of fitting to the noise). Both HCFC-142b and HFC-43-10mee have significant spread in the calculated concentration profiles, roughly similar to the spread

10 in CH_3CCl_3 and HFC-134a in Fig. 8 (relative to their overall range of concentration in the NEEM firm), suggesting that they would be useful additional tracers for calibrating diffusivity above the lock-in depth at NEEM. HFC-43-10mee has a larger concentration gradient in the upper firm (relative to its overall range) than any of the other tracers modelled for NEEM, and we do see a larger spread in concentration around 20 m for

15 the calculated HFC-43-10mee than for any other tracers in Fig. 8, so a tracer with an atmospheric history like this would be worth including for calibration. HCFC-142b has a depth profile more like HFC-134a, so may not be as useful as an additional reference tracer. The value of any new tracers will clearly depend on how accurately they can be measured and how certain their atmospheric history is, relative to their variation with

20 depth.

3.4 DE08-2

Figure 10 shows results for the DE08-2 firm. The lowest value of Φ that the GA finds for these observations is 0.64, and we consider solutions up to $\Phi = 0.8$ corresponding to a confidence level of 68 %. The solution with the lowest Φ has diffusion reduced

25 by 89 % over the melt layer, a bit larger than the reduction of about 80 % found by Trudinger et al. (1997). Most of the representative solutions have reduction of mixing in the range 85–92 %, however there are two solutions with reduction around 50 %.

The DE08-2 lock-in depth is around 73m based on the change in slope of the concentration measurements, and our molecular diffusion extends well below this depth. We have some solutions with $\Phi < 0.8$ that have molecular diffusion of around $1.0 \text{ m}^2 \text{ yr}^{-1}$ for a significant part of the lock-in zone.

3.5 DSSW20K

Figure 11 shows results for DSSW20K. The lowest Φ found was 0.91, and we consider Φ up to 1.08 corresponding to a confidence level of 68 %. We again see some molecular diffusion extending below the lock-in depth, although the range of depths over which our representative solutions have (molecular) diffusion stopping is smaller than for NEEM or DE08-2. We used exponentially-decreasing eddy diffusion to model convective mixing near the surface. As we discuss in more detail in the section on dispersive mixing in the Supplement, the parameters for the exponentially-decreasing eddy diffusion profile preferred by the model lead to significant eddy diffusion in the lock-in zone (this was not the case for NEEM).

In Trudinger et al. (2002) and also here, modelled CO_2 at the bottom of the firn is lower than observed, and our best case does not match the $^{14}\text{CO}_2$ peak particularly well. In Sturrock et al. (2002) we had a discrepancy between the DSSW20K firn measurements of CFC-113, CFC-115 and halons H-1211 and H-1301 dated with the old CSIRO firn model and the atmospheric record from the Cape Grim Air Archive. We find that this discrepancy has disappeared with the new version of the CSIRO firn model and our best set of diffusivity parameters for DSSW20K, most likely because we are now including the upward flow of air due to compression. The values of γ_X that we use here differ from the values used in Sturrock et al. (2002), but the difference is too small to explain the discrepancy.

Between about 30–38 m, there is greater spread in the calculated concentrations of many of the tracers than in other parts of the firn. This is a consequence of the gap of more than 10 m between sampling depths for most tracers. Although this region is above the lock-in depth of 43 m, the diffusivity decreases by at least factor of 10 over

Constraining firn diffusivity

C. M. Trudinger et al.

Title Page

Abstract

Introduction

Conclusions

References

Tables

Figures

◀

▶

◀

▶

Back

Close

Full Screen / Esc

Printer-friendly Version

Interactive Discussion



Constraining firn diffusivity

C. M. Trudinger et al.

[Title Page](#)[Abstract](#)[Introduction](#)[Conclusions](#)[References](#)[Tables](#)[Figures](#)[◀](#)[▶](#)[◀](#)[▶](#)[Back](#)[Close](#)[Full Screen / Esc](#)[Printer-friendly Version](#)[Interactive Discussion](#)

this depth range. The sampling depths at DSSW20K were chosen to give priority to measurements in the lock-in zone, to provide most samples of the oldest air while still giving some samples through the diffusive part of the firn to constrain diffusion there. More sampling depths, particularly in the 10 m above the lock-in zone, would most likely reduce the uncertainty in diffusion in that region. In the section on dispersive mixing in the Supplement, we see significant spread in isotopic fractionation of $\delta^{13}\text{CO}_2$ due to diffusion through this region, which might also be reduced by more samples. The extent to which reduction of uncertainty in diffusion in this region affects the uncertainty in concentrations or effective ages in the lock-in zone for different tracers (because air in the lock-in zone has been influenced by diffusion throughout the firn column) could be assessed with a pseudo-data study.

3.6 South Pole

Figure 12 shows results from South Pole 1995. The best Φ obtained was 0.92, and we consider solutions up to $\Phi = 1.0$ which corresponds to a confidence level of 68 %. We currently do not include thermal diffusion (Severinghaus et al., 2001) in the CSIRO firn model, so have excluded $\delta^{15}\text{N}_2$ observations near the surface that are affected by thermal diffusion. Even without using the lower measurements of SF_6 , CFCs, and CH_3CCl_3 for calibration, the spread of representative solutions for these tracers is quite small, and in good agreement with the observations. These observations could be used with increased uncertainties, however any errors are likely to be systematic rather than random, and could also be correlated between species.

Figure 13 shows results from South Pole 2001. Our best Φ is 1.24. We consider solutions up to $\Phi = 1.38$ corresponding to a confidence level of 68 %.

3.7 Comparison of sites

In Fig. 14 we show CO_2 age distributions and spectral width variation with depth for NEEM, DE08-2, DSSW20K, South Pole 1995 and South Pole 2001. The ranges for all

sites correspond to a 68 % confidence level (i.e. 1σ). The age distributions for all sites correspond to depths (indicated on the plots) where CO_2 has a mean age of about 1940. DE08-2 only contains firn air with CO_2 age back to about 1978, so we have calculated the age distribution in trapped air for DE08-2.

Although we treat South Pole 1995 and 2001 as separate sites, most of the difference between their age distributions in Fig. 14 is probably due to calibrating with different tracers. The age distribution above 50 m is more tightly constrained for South Pole 1995 than South Pole 2001, presumably because of the extra tracers at South Pole 1995. South Pole 1995 has a wider range of uncertainty below 115 m than South Pole 2001, but the two sites have used similar measurements in this region, so the reason for the difference is not clear.

Of the sites we have modelled, DE08-2 ice has the narrowest age spread at 1940 (with a best estimate of the spectral width of 4.5 years and a 1σ range of 4.4 to 4.7 yr), followed by DSSW20K firn (7.0 yr with a 1σ range of 6.5–8.5 yr), NEEM firn (10.8 yr with a 1σ range of 9.6–11.3 yr) then South Pole firn (the 1995 site has a best estimate of 16.0 yr with a 1σ range of 15.7–18.9 yr and the 2001 site has a best estimate of 18.1 yr and a 1σ range of 17.2–18.2 yr). We have applied our model and calibration technique to several sites with quite different properties and tracers available for calibration. All sites that we modelled required some diffusion in the lock-in zone.

3.8 Inferring relative diffusion coefficients

We repeated the Synthetic A and B Subset Ten calculations estimating the relative diffusion coefficients, γ_X , of seven tracers in addition to the diffusivity profile and well-mixed layer depth. We allowed a range for the diffusion coefficients of $\pm 10\%$ of the true value. Sensitivity tests showed that $\delta^{15}\text{N}_2$ varies very little when $\gamma_{15\text{N}_2}$ is varied within this range, so we did not try to estimate it; we also did not try to estimate $\gamma_{14}\text{CO}_2$, but included observations of these two tracers and used their true values of γ_X . The weighted RMS mismatch from noisy Synthetic A and B observations and truth are given for the best solutions in Table 3 (denoted TenDC). In the Supplement we show

Constraining firn diffusivity

C. M. Trudinger et al.

Title Page

Abstract

Introduction

Conclusions

References

Tables

Figures

◀

▶

◀

▶

Back

Close

Full Screen / Esc

Printer-friendly Version

Interactive Discussion



scatter plots of diffusion coefficients against Φ for all solutions tested by the GA that had $\Phi_A < 1.25$ for Synthetic A and $\Phi_B < 1.0$ for Synthetic B.

For most tracers the Synthetic A case gives a greater mismatch from the noisy concentration observations and from the true concentrations than Subset Ten with the true relative diffusion coefficients. This is probably because we are now estimating a larger number of parameters (23), and it has become harder for the GA to locate the true solution. The solution with the lowest Φ_A has estimated relative diffusion coefficients that are between 0.9 % too low and 2.4 % too high.

For Synthetic B, the best solution for most tracers is closer to the noisy observations but further from the truth than the case with known diffusion coefficients. The best case has diffusion coefficients between 2.1 % too low and 8.4 % too high. CFC-11 in particular has an estimated diffusion coefficient that is very high, and it is the tracer with the largest systematic errors added (apart from $\delta^{15}\text{N}_2$ and $^{14}\text{CO}_2$ for which we're not estimating γ_X), see the first column in Table 3.

The Synthetic A calculation does quite a good job at estimating γ_X , particularly as we are now estimating 23 parameters at once. Most of the best estimates of γ_X are slightly high, but there is only one tracer tying them together (CO_2), so we might expect a slightly lower CO_2 diffusivity versus depth profile compared to the truth to compensate. The Synthetic B results are more concerning, as the estimates are further from the true γ_X and often outside the $\pm 2\%$ range quoted for the Matsunaga et al. (1993, 1998, 2002) values.

We repeated the calibrations for NEEM, DE08-2 and DSSW20K with relative diffusion coefficients estimated along with the other parameters. For NEEM, we recalibrated Subsets Ten and TenEddy estimating relative diffusion coefficients, and results are shown as columns TenDC and TenEddyDC in Table 4). The best cases had Φ_N significantly lower than the values obtained with fixed diffusion coefficients ($\Phi_N = 0.66$ compared to 0.74 with fixed γ_X for TenEddy). There was most reduction in mismatch for SF_6 and CFC-12. The best case had relative diffusion coefficients ranging from 11 % higher to 8 % lower than the values given in Buizert et al. (2012). CH_4 and CFC-12 had

Constraining firm diffusivity

C. M. Trudinger et al.

Title Page

Abstract

Introduction

Conclusions

References

Tables

Figures

◀

▶

◀

▶

Back

Close

Full Screen / Esc

Printer-friendly Version

Interactive Discussion



the greatest change, with the best Φ_N obtained with lower values of relative diffusion coefficient, as well as a higher value for SF₆.

Figure 15 shows the results for all three sites, adjusted to apply to a temperature of 244.25 K. We started with a range of $\pm 10\%$ of the Matsunaga et al. (1993, 1998, 2002) values (shown by the error bars in Fig. 15), but if the GA preferred a solution at the boundary we extended the range and reran the calculation. To the left of each of the error bars, we show various published estimates (measured and empirical) of γ_X for eight tracers. To the right of the error bars are the values we determined using the GA for the five firn sites (NEEM is included twice, using both methods for convective mixing near the surface, to test the stability of these results). These values give a better fit to the observations than using the Matsunaga et al. (1993, 1998, 2002) γ_X , however we do not know whether the different values of γ_X are compensating for other errors, such as in the atmospheric history or missing or incorrectly modelled processes in the firn model. Scatter plots of relative diffusion coefficients as a function of Φ in each case show a clear preference for particular values of relative diffusion coefficient, and often (although not always) a fairly steep increase in Φ as you move away from that value.

In some cases the values estimated by the GA are close to the Matsunaga et al. (1993, 1998, 2002) values, but in other cases they are significantly different. It is difficult to trust these results after the Synthetic B calculations, if we assume that real observations could suffer from similar systematic error. If Matsunaga et al. (1993, 1998, 2002) are correct that their diffusion coefficients are accurate to $\pm 2\%$, then their values are more reliable than our calibrated estimates, certainly at present.

However, an uncertainty of even $\pm 2\%$ for the diffusion coefficients estimated by Matsunaga et al. (1993, 1998, 2002), and probably higher for other tracers not estimated by Matsunaga et al. (1993, 1998, 2002) such as CH₃CCl₃ and HCFC-141b, will contribute to the overall uncertainty in the inferred diffusivity profile and therefore the uncertainty in atmospheric reconstructions. One way to account for this uncertainty would be to include relative diffusion coefficients in the GA calibration, as we have already done, but with a range of $\pm 2\%$ (or greater for some tracers) for the purpose of taking account

Constraining firn diffusivity

C. M. Trudinger et al.

Title Page

Abstract

Introduction

Conclusions

References

Tables

Figures

◀

▶

◀

▶

Back

Close

Full Screen / Esc

Printer-friendly Version

Interactive Discussion



of their uncertainty rather than to improve the estimates of their values. We would probably prefer to use as our best solution a case with the Matsunaga et al. (1993, 1998, 2002) values of γ_X , even though other values of γ_X might give a lower Φ , but we could easily include some additional members in our representative ensemble that have these other values of γ_X to reflect this component of the uncertainty. As firm measurements and models become more accurate this may become a relatively more important contribution to the overall uncertainty.

3.9 Dispersion in the lock-in zone

In the Supplement we look in detail at dispersion in the lock-in zone; the results are summarised here. We first tested the sensitivity of our modelled concentrations to lock-in zone dispersion by simply adding a dispersive transport term to the forward model (which had been calibrated without dispersion). Of the sites and tracers we modelled, NEEM was most sensitive to adding dispersion, particularly for $^{14}\text{CO}_2$ and CH_3CCl_3 . At the other sites, adding lock-in zone dispersion had no significant impact on the modeled profiles. This is probably because we already have significant diffusion in the lock-in zone – in most cases the diffusion is molecular, although DSSW20K had significant eddy diffusion from the surface convection extending into the lock-in zone. Given the lack of sensitivity of the tracers, it would be difficult to constrain lock-in zone dispersion in the model at these sites.

As a second test we added dispersive mixing to calibrations with NEEM synthetic observations, estimating parameters for dispersion for two cases: one with dispersion in the forward run to generate the synthetic data, and one without. We were able to recover roughly the correct dispersion profile in both cases. These calculations were equivalent to the Synthetic A cases with small, Gaussian noise. While there was information in these observations to distinguish between molecular and dispersive mixing in the lock-in zone, observations with realistic errors would be expected to reduce the ability of the calibration algorithm to discern between molecular diffusion and dispersive transport.

Constraining firm diffusivity

C. M. Trudinger et al.

Title Page

Abstract

Introduction

Conclusions

References

Tables

Figures

◀

▶

◀

▶

Back

Close

Full Screen / Esc

Printer-friendly Version

Interactive Discussion



Constraining firn diffusivity

C. M. Trudinger et al.

[Title Page](#)[Abstract](#)[Introduction](#)[Conclusions](#)[References](#)[Tables](#)[Figures](#)[◀](#)[▶](#)[◀](#)[▶](#)[Back](#)[Close](#)[Full Screen / Esc](#)[Printer-friendly Version](#)[Interactive Discussion](#)

Whether or not diffusive transport occurs is mostly of importance for predicting the amount of diffusive isotopic fractionation in the firn column. Therefore, as a third test we recalibrated the model for DSSW20K including dispersion as well as molecular diffusivity, for each of the two methods for modelling convective mixing near the surface. We then calculated the isotopic diffusion correction for fractionation of $\delta^{13}\text{CO}_2$ at DSSW20K. The range in the diffusion correction for a confidence level of 68 % increased when we allowed for dispersion. The increase in range was very depth dependent, and was mostly an increase of between 1.5 and 3 times but did reach a factor of 7 times just before the lock-in depth. In absolute terms, the maximum $\delta^{13}\text{CO}_2$ diffusion correction at DSSW20K was 0.15 ‰ (both with and without dispersion), with a maximum difference between the best estimate and the representative solution most different from the best estimate of 0.04 ‰.

In general, allowing for dispersion increases the equifinality. Even if we cannot resolve it in model calibration, if evidence of it occurring continues to grow then we should include multiple solutions that include this possibility in order to estimate the uncertainty range. This uncertainty will be of particular importance for reconstructions of trace gas isotopes from ice core and firn air data.

4 Discussion

The ability of a reference tracer to constrain the diffusivity profile depends on two things. The first is the amount of variation with depth the tracer has in the firn, which is largely a consequence of the particular atmospheric history of the tracer, but also depends on the processes in the firn that we wish to learn about. The second is the total uncertainty in the data, based on analytical precision, atmospheric reconstructions, possibility of contamination etc. The first is about the signal and how much information on firn processes is contained in the depth profiles of each of the reference tracers, the second is about the noise and how much this obscures the signal. Analysis of both the signal and the noise are important for determining which tracers are most useful, as is the

case with any inverse study. As discussed below, tracers will differ from site to site in their relative importance, depending on the relative timescales of atmospheric change and firn closure.

We have seen that some tracers constrain diffusivity more than others. In particular, tracers with more variation through the diffusive part of the firn, like CH_3CCl_3 , HFC-134a, SF_6 and HFC-43-10mee are most useful for constraining diffusivity in this region. Similarly tracers with most variation in the lock-in zone, like $^{14}\text{CO}_2$ (at NEEM), CO_2 and CH_4 , constrain diffusion most there. Tracers with constant concentration over parts of the firn are not so useful in those regions (such as CH_4 through the diffusive part). These conclusions do not account for data errors, and the larger the error is for a particular tracer, the less useful it becomes, particularly if the noise is correlated.

The assumption that diffusivity decreases monotonically with depth has a significant impact on our results, most particularly the range of solutions that are found for a given threshold of Φ . Without this assumption or any other smoothness constraint, the equifinality could increase almost without bound, as many oscillatory solutions are then permitted, as shown by Rommelaere et al. (1997). The assumption is certainly reasonable and consistent with other assumptions that we have made, such as the density and open porosity being time invariant and monotonic with depth.

Using a larger number of tracers does constrain diffusivity more tightly, as has always been assumed. However, in terms of the signal, it appears that three carefully chosen tracers will do nearly as well as ten tracers in constraining (only) molecular diffusivity if the noise is small and Gaussian, and if we assume a monotonic diffusivity. Small improvements may occur with each different tracer that is added. We can quantify how much additional constraint, and for which regions of the firn, is provided by each extra tracer by comparing the spread of solutions with and without the extra tracers.

In terms of the noise, obviously the larger the noise the more it will overwhelm the signal, and systematic errors are more difficult to deal with than random errors. In the synthetic calculations, we chose data errors to be proportional to the range of concentrations covered by the firn measurements. Actual data errors will vary widely

Constraining firn diffusivity

C. M. Trudinger et al.

Title Page

Abstract

Introduction

Conclusions

References

Tables

Figures

◀

▶

◀

▶

Back

Close

Full Screen / Esc

Printer-friendly Version

Interactive Discussion



relative to this range, and this will affect which tracers have more information on firn processes. Overfitting noisy data was a problem for up to three tracers with a small amount of normally-distributed noise, and more of a problem with systematic noise. If systematic noise is related for different tracers, overfitting the data will be harder to avoid.

What matters for a particular site is the timing of features in the atmospheric records relative to the range of air ages in the firn column at the sampling date, so the relative value of different tracers is expected to vary for different sites and drilling dates. For example, the bomb pulse in $^{14}\text{CO}_2$ can be a very useful signal, but this will depend on where it is in the firn, such as above or below the lock-in depth. At some time in the future, the peak in CH_3CCl_3 will move into the lock-in zone for some sites, so will then provide a useful tracer to constrain lock-in zone diffusion. It will eventually move into trapped bubbles in ice, where it might be useful to help constrain trapping in addition to firn diffusion. Tracers that have been useful in the past for constraining firn diffusivity may not be as useful in the future, but the principles for choosing tracers will remain the same.

Based on our study, the recommendation for future firn campaigns would be to give priority to tracers that have most variation with depth (relative to their uncertainties) in different parts of the firn. $\delta^{15}\text{N}_2$ is useful for constraining parameters related to convective mixing, and CH_3CCl_3 and $^{14}\text{CO}_2$ have also been particularly useful. The more tracers that can be measured, and with good characterisation of their uncertainties, the less chance there will be of overfitting noise. There is value in making as many measurements as possible through the firn column, with particular emphasis on the lock-in zone and the 10 m or so above the lock-in depth where diffusivity changes rapidly with depth.

We modelled convective mixing near the surface in two different ways – with a well-mixed layer and exponentially-decreasing eddy diffusion. For NEEM and DSSW20K where we tried each of these methods, the overall fit to calibration observations was very similar (differences in Φ of only 0.01 for NEEM and 0.04 for DSSW20K), with the

Constraining firn diffusivity

C. M. Trudinger et al.

[Title Page](#)[Abstract](#)[Introduction](#)[Conclusions](#)[References](#)[Tables](#)[Figures](#)[◀](#)[▶](#)[◀](#)[▶](#)[Back](#)[Close](#)[Full Screen / Esc](#)[Printer-friendly Version](#)[Interactive Discussion](#)

exponential eddy diffusion method always slightly better. Cases using each of these methods could be included in a representative set of diffusivity parameters.

Of the three types of uncertainty discussed in the Introduction, we found that all types were important. Most of our calculations involved estimating only molecular diffusivity and a well mixed layer depth. In this case we found that the uncertainty due to data uncertainties was more important than equifinality beyond a few carefully selected tracers (as long as we allow only monotonic diffusivity profiles). However, when we added additional processes such as dispersion in an attempt to take account of uncertainties in model structure, equifinality became more important. In that case, different types of tracers might be needed to reduce the equifinality (e.g. isotopic ratios might be the best way to learn about dispersion in the lock-in zone).

How important the uncertainties are depends on what we are doing with the model. Reconstructing the atmospheric history of a tracer that has a similar history to a tracer used for calibration would be expected to have a small uncertainty (this would be the case for CCl_4 as shown for NEEM). In contrast, an estimate of the diffusive fractionation affecting isotopic ratios might have large uncertainty (we saw this for $\delta^{13}\text{CO}_2$ at DSSW20K). As the number of observations increases, the confidence level associated with a chosen threshold increases, but if important processes are missing from the model, we may seriously underestimate the errors in a model prediction.

The firm model intercomparison by Buizert et al. (2012) showed one result each from six different firm models, with some variation in the processes that were included, most notably dispersion in the lock-in zone. Here we looked at multiple solutions compatible with the observations over the same range of model-data mismatch with only one firm model. The range of results we obtained for NEEM case TenEddy for a similar range of Φ was not far from that obtained with the six models. The range in spectral width of the CO_2 age distribution at 78 m in Buizert et al. (2012) was 8.3–12.5 yr, compared to the range we obtain at the same depth (with $\Phi_N < 0.93$) of 8.4–12.8 yr (without dispersion). We also calculated a range for Diagnostic 1 in Buizert et al. (2012) (that quantifies isotopic fractionation) of about 0.025‰ at 70 m and 0.04‰ at 80 m, compared with

Constraining firm diffusivity

C. M. Trudinger et al.

Title Page

Abstract

Introduction

Conclusions

References

Tables

Figures

◀

▶

◀

▶

Back

Close

Full Screen / Esc

Printer-friendly Version

Interactive Discussion



that from the six models of about 0.04‰ at 70 m and 0.05‰ at 80 m. The uncertainty ranges from our study and Buizert et al. (2012) are both important, but not independent. If we include the equifinality due to uncertain processes like dispersion in one firm model it should cover some of the range covered by different models, but there may still be other differences between models that will not be captured with one model alone. Part of the difference between the models in Buizert et al. (2012) will be due to the fact that a single solution from each model was compared, whereas we would expect that there will be multiple solutions that fit the observations almost as well as the best cases, as we have found here, and these will probably have overlapping ranges to some extent. However, both this work and the intercomparison suggest that the use of a single calculation with one firm model for reconstruction of atmospheric records is not adequate to capture the uncertainty due to equifinality, which should include uncertainty in firm processes.

5 Conclusions

We have developed a new version of the CSIRO firm model and used it to test how well different tracers constrain the firm diffusivity profile, one of the most important and uncertain of the required model inputs. Our method for reconstructing the profile of molecular diffusivity in firm based on the genetic algorithm and monotonic splines was successful in two synthetic cases with different error characteristics. When calibrating the model, we generate an ensemble of representative diffusivity parameter sets that all fit the calibration data adequately. This ensemble represents the uncertainty in the model due to data uncertainty, equifinality and in some cases uncertainty in model processes.

The best tracers for calibrating molecular diffusivity in firm are those with most variation with depth relative to their uncertainties. In a synthetic case for NEEM with small, Gaussian errors, CH₃CCl₃ and HFC-134a were particularly useful above the lock-in zone and ¹⁴CO₂ below the lock-in zone. δ¹⁵N is useful for constraining parameters

Constraining firm diffusivity

C. M. Trudinger et al.

Title Page

Abstract

Introduction

Conclusions

References

Tables

Figures

◀

▶

◀

▶

Back

Close

Full Screen / Esc

Printer-friendly Version

Interactive Discussion



related to convective mixing near the surface. It appears that three carefully selected tracers will do almost as well as a larger number of tracers in terms of constraining molecular diffusivity alone when data errors are small and Gaussian, however with either realistic data errors or the need to constrain additional processes there is benefit to including as many tracers as possible. Overfitting of noisy data is a problem even for purely random noise and a more serious problem for systematic errors.

We have applied our model and calibration technique to several sites with quite different properties and tracers available for calibration. All of the sites we modelled had non-zero diffusion below the lock-in depth, of the order of $0.1\text{--}1.0\text{ m}^2\text{ yr}^{-1}$. The inclusion of the upward flow of air due to compression in the new version of the CSIRO firm model is clearly important. Although diffusivity can compensate for its absence to some extent, we are now able to match observations better with the upward flow.

This work has not been a comprehensive assessment of all uncertainties affecting firm models, but an attempt to quantify uncertainties due mainly to data uncertainties and equifinality. Our calculations for convective mixing and dispersion in the lock-in zone are a start to including the effects of uncertainty in model processes. We challenge the idea of a single firm model with one parameter set, instead suggesting the use of multiple parameter sets, preferably with multiple representations of uncertain processes. Uncertainty due to equifinality does reduce as more tracers are used for model calibration, but it does not disappear completely, particularly if we allow for processes like dispersion in the lock-in zone. When firm models are used to reconstruct atmospheric histories, it is important to take into account the uncertainty due to equifinality, including the uncertainty in relative diffusion coefficients.

Supplementary material related to this article is available online at:
[http://www.atmos-chem-phys-discuss.net/12/17773/2012/
acpd-12-17773-2012-supplement.pdf](http://www.atmos-chem-phys-discuss.net/12/17773/2012/acpd-12-17773-2012-supplement.pdf).

**Constraining firm
diffusivity**

C. M. Trudinger et al.

Title Page

Abstract

Introduction

Conclusions

References

Tables

Figures

◀

▶

◀

▶

Back

Close

Full Screen / Esc

Printer-friendly Version

Interactive Discussion



Acknowledgements. This work has been undertaken as part of the Australian Climate Change Science Program, funded jointly by the Department of Climate Change and Energy Efficiency, the Bureau of Meteorology and CSIRO. CSIRO's research in this area was also funded by the Centre for Ice and Climate at the University of Copenhagen. The Centre of Excellence of Mathematics and Statistics of Complex Systems (MASCOS) has been funded by the Australian Research Council. I. Enting's fellowship at MASCOS was funded in part by CSIRO. P. Rayner is in receipt of an Australian Professorial Fellowship (DP1096309) C. Buizert was supported by the NOAA Climate and Global Change Fellowship Program, administered by the University Corporation for Atmospheric Research. We thank Patricia Martinerie for useful discussions and sharing atmospheric histories, Jeff Severinghaus for advice on equations for eddy diffusion and Mark Battle for providing data and advice for the South Pole firn sites. We acknowledge Ben Miller (now at CIRES/University of Colorado) for the Cape Grim Air Archive measurements of HCFC-141b used in this work.

References

- Andrussow, L., Bartels, J., Eucken, A., Hellwege, K. H., and Schäfer, K.: Transportphänomene I (Viskosität und Diffusion), in: *Eigenschaften der Materie in ihren Aggregatzuständen*, 5. Teil, Bandteil a.; Landolt-Börnstein: Zahlenwerte und Funktionen aus Physik, Chemie, Astronomie, Geophysik und Technik, vol. 6, Springer Verlag, Berlin, 1969. 17788
- Árnadóttir, T. and Segall, P.: The 1989 Loma Prieta earthquake imaged from inversion of geodetic data, *J. Geophys. Res.*, 99, 21835–21855, 1994. 17782
- Aydin, M., Saltzman, E. S., De Bruyn, W. J., Montzka, S. A., Butler, J. H., and Battle, M.: Atmospheric variability of methyl chloride during the last 300 years from an Antarctic ice core and firn air, *Geophys. Res. Lett.*, 31, L02109, doi:10.1029/2003GL018750, 2004. 17787
- Battle, M., Bender, M., Sowers, T., Tans, P. P., Butler, J. H., Elkins, J. W., Ellis, J. T., Conway, T., Zhang, N., Lang, P., and Clarke, A. D.: Atmospheric gas concentrations over the past century measured in air from firn at the South Pole, *Nature*, 383, 231–235, 1996. 17787
- Beven, K.: A manifesto for the equifinality thesis, *J. Hydrol.*, 320, 18–36, 2006. 17776
- Buizert, C., Martinerie, P., Petrenko, V. V., Severinghaus, J. P., Trudinger, C. M., Witrant, E., Rosen, J. L., Orsi, A. J., Rubino, M., Etheridge, D. M., Steele, L. P., Hogan, C., Laube, J. C., Sturges, W. T., Levchenko, V. A., Smith, A. M., Levin, I., Conway, T. J., Dlugokencky, E. J.,

Constraining firn diffusivity

C. M. Trudinger et al.

Title Page

Abstract

Introduction

Conclusions

References

Tables

Figures

◀

▶

◀

▶

Back

Close

Full Screen / Esc

Printer-friendly Version

Interactive Discussion



**Constraining firm
diffusivity**

C. M. Trudinger et al.

Title Page

Abstract

Introduction

Conclusions

References

Tables

Figures

◀

▶

◀

▶

Back

Close

Full Screen / Esc

Printer-friendly Version

Interactive Discussion



Lang, P. M., Kawamura, K., Jenk, T. M., White, J. W. C., Sowers, T., Schwander, J., and Blunier, T.: Gas transport in firm: multiple-tracer characterisation and model intercomparison for NEEM, Northern Greenland, *Atmos. Chem. Phys.*, 12, 4259–4277, doi:10.5194/acp-12-4259-2012, 2012. 17776, 17778, 17782, 17783, 17784, 17785, 17787, 17788, 17789, 17796, 17802, 17808, 17809, 17827

Butler, J. H., Battle, M., Bender, M. L., Montzka, S. A., Clarke, A. D., Saltzman, E. S., Sucher, C. M., Severinghaus, J. P., and Elkins, J. W.: A record of atmospheric halocarbons during the twentieth century from polar firn, *Nature*, 399, 749–755, 1999. 17787, 17788

Butler, J. H., Montzka, S. A., Battle, M., Clarke, A. D., Mondeel, D. J., Lind, J. A., Hall, B. D., and Elkins, J. W.: Collection and Analysis of Firn Air from the South Pole, 2001, AGU Fall Meeting Abstracts, p. F145, 2001. 17787

Chen, N. H. and Othmer, D. F.: New generalized equation for gas diffusion coefficient, *J. Chem. Eng. Data*, 7, 37–41, 1962. 17788, 17834

Colbeck, S. C.: Air movement in snow due to windpumping, *J. Glaciol.*, 35, 209–213, 1989. 17775

Craig, H., Horibe, Y., and Sowers, T.: Gravitational separation of gases and isotopes in polar ice caps, *Science*, 242, 1675–1678, 1988. 17775

Draper, N. R. and Smith, H.: *Applied Regression Analysis*, Wiley, New York, 1981. 17782

Etheridge, D. M. and Wookey, C. W.: Ice core drilling at a high accumulation area of Law Dome, Antarctica, 1987, in: *Ice Core Drilling, Proceedings of the Third International Workshop on Ice Core Drilling Technology*, Grenoble, France, October 10–14 1988, edited by: Rado, C. and Beaudoin, D., 86–96, Centre Natl. de la Rech. Sci., Grenoble, 1989. 17786

Etheridge, D. M., Steele, L. P., Langenfelds, R. L., Francey, R. J., Barnola, J. M., and Morgan, V. I.: Natural and anthropogenic changes in atmospheric CO₂ over the last 1000 years from air in Antarctic ice and firn, *J. Geophys. Res.*, 101, 4115–4128, 1996. 17785, 17786

Etheridge, D. M., Steele, L. P., Francey, R. J., and Langenfelds, R. L.: Atmospheric methane between 1000 AD and present: evidence for anthropogenic emissions and climate variability, *J. Geophys. Res.*, 103, 15979–15993, 1998. 17785

Fabre, A., Barnola, J. M., Arnaud, L., and Chappellaz, J.: Determination of gas diffusivity in polar firn: comparison between experimental measurements and inverse modeling, *Geophys. Res. Lett.*, 27, 557–560, 2000. 17775, 17776

Constraining firm diffusivity

C. M. Trudinger et al.

Title Page

Abstract

Introduction

Conclusions

References

Tables

Figures

◀

▶

◀

▶

Back

Close

Full Screen / Esc

Printer-friendly Version

Interactive Discussion



- Freitag, J., Dobrindt, U., and Kipfstuhl, J.: A new method or predicting transport properties of polar firm with respect to gases in the pore-space scale, *Ann. Glaciol.*, 35, 538–544, 2002. 17775
- Freitag, J., Wilhelms, F., and Kipfstuhl, S.: Microstructure-dependent densification of polar firm derived from X-ray microtomography, *Ann. Glaciol.*, 50, 243–250, 2004. 17775
- Fuller, E. N., Schettler, P. D., and Giddings, J. C.: A new method for prediction of binary gas-phase diffusion coefficients, *Ind. Eng. Chem.*, 58, 19–27, 1966. 17788, 17834
- Haupt, R. and Haupt, S.: *Practical Genetic Algorithms*, John Wiley and Sons, 1998. 17780
- Højberg, A. L. and Refsgaard, J. C.: Model uncertainty-parameter uncertainty versus conceptual models, *Water Sci. Technol.*, 52, 177–186, 2005. 17776
- Huber, C., Beyerle, U., Leuenberger, M., Schwander, J., Kipfer, R., Spahni, R., Severinghaus, J. P., and Weiler, K.: Evidence for molecular size dependent gas fractionation in firm air derived from noble gases, oxygen, and nitrogen measurements, *Earth Planet. Sci. Lett.*, 243, 61–73, 2006. 17775
- Kawamura, K., Severinghaus, J. P., Ishidoya, S., Sugawara, S., Hashida, G., Motoyama, H., Fujii, Y., Aoki, S., and Nakazawa, T.: Convective mixing of air in firm at four polar sites, *Earth Planet. Sci. Lett.*, 244, 672–682, doi:10.1016/j.epsl.2006.02.017, 2006. 17775
- Levchenko, V. A., Etheridge, D. M., Francey, R. J., Trudinger, C. M., Tuniz, C., Lawson, E. M., Smith, A. M., Jacobsen, G. E., Hua, Q., Hotchkis, M. A. C., Fink, D., Morgan, V., and Head, J.: Measurements of the $^{14}\text{CO}_2$ bomb pulse in firm and ice at Law Dome, Antarctica, *Nucl. Instr. Meth. B*, 123, 290–295, 1997. 17786
- Lugg, G. A.: Diffusion coefficients of some organic and other vapor in air, *Anal. Chem.*, 40, 1072–1077, 1968. 17788, 17834
- Marrero, T. R. and Mason, E. A.: Gaseous diffusion coefficients, *J. Phys. Chem. Ref. Data*, 1, 3–116, doi:10.1063/1.3253094, 1972. 17788, 17834
- Martinerie, P., Nourtier-Mazauric, E., Barnola, J.-M., Sturges, W. T., Worton, D. R., Atlas, E., Gohar, L. K., Shine, K. P., and Brasseur, G. P.: Long-lived halocarbon trends and budgets from atmospheric chemistry modelling constrained with measurements in polar firm, *Atmos. Chem. Phys.*, 9, 3911–3934, doi:10.5194/acp-9-3911-2009, 2009. 17788, 17828
- Matsunaga, N., Hori, M., and Nagashima, A.: Mutual diffusion coefficients of halogenated hydrocarbon refrigerant-air systems, *High Temp.-High Press.*, 25, 185–192, 1993. 17783, 17788, 17802, 17803, 17804, 17834

Constraining firn diffusivity

C. M. Trudinger et al.

Title Page

Abstract

Introduction

Conclusions

References

Tables

Figures

◀

▶

◀

▶

Back

Close

Full Screen / Esc

Printer-friendly Version

Interactive Discussion



Matsunaga, N., Hori, M., and Nagashima, A.: Diffusion coefficients of global warming gases into air and its component gases, *High Temp.-High Press.*, 30, 77–83, 1998. 17783, 17788, 17802, 17803, 17804, 17834

Matsunaga, N., Hori, M., and Nagashima, A.: Measurements of the mutual diffusion coefficients of gases by the Taylor method, 7th report, measurements on the SF₆-air, SF₆-N₂, SF₆-O₂, CFC12-N₂, CFC12-O₂, HCFC22-N₂ and HCFC22-O₂ systems, *Trans. Jpn. Soc. Mech. Eng. B.*, 68, 550–555, 2002. 17783, 17788, 17802, 17803, 17804, 17834

Meinshausen, M., Smith, S., Calvin, K., Daniel, J., Kainuma, M., Lamarque, J.-F., Matsumoto, K., Montzka, S., Raper, S., Riahi, K., Thomson, A., Velders, G., and van Vuuren, D.: The RCP greenhouse gas concentrations and their extensions from 1765 to 2300, *Climatic Change*, 109, 213–241, doi:10.1007/s10584-011-0156-z, 2011. 17828

Rommelaere, V., Arnaud, L., and Barnola, J.: Reconstructing recent atmospheric trace gas concentrations from polar firn and bubbly ice data by inverse methods, *J. Geophys. Res.*, 102, 30069–30083, 1997. 17775, 17776, 17778, 17788, 17793, 17806

Schwander, J.: The transformation of snow to ice and the occlusion of gases, in: *The Environmental Record in Glaciers and Ice Sheets*, edited by: Oeschger, H. and Langway, C. C., John Wiley, New York, 53–67, 1989. 17775

Schwander, J., Stauffer, B., and Sigg, A.: Air mixing in firn and the age of the air at pore close-off, *Ann. Glaciol.*, 10, 141–145, 1988. 17775

Schwander, J., Barnola, J. M., Andrié, C., Leuenberger, M., Ludin, A., Raynaud, D., and Stauffer, B.: The age of the air in the firn and the ice at Summit, Greenland, *J. Geophys. Res.*, 98, 2831–2838, 1993. 17775, 17788

Seber, G. A. F. and Wild, C. J.: *Nonlinear Regression*, Wiley, doi:10.1002/0471725315, 2005. 17782

Severinghaus, J. P., Grachev, A., and Battle, M.: Thermal fractionation of air in polar firn by seasonal temperature gradients, *Geochem. Geophys. Geosyst.*, 2, 1048, doi:10.1029/2000GC000146, 2001. 17775, 17778, 17796, 17800

Severinghaus, J. P., Albert, M. R., Courville, Z. R., Fahnestock, M. A., Kawamura, K., Montzka, S. A., Mühle, J., Scambos, T. A., Shields, E., Shuman, C. A., Suwa, M., Tans, P., and Weiss, R. F.: Deep air convection in the firn at a zero-accumulation site, Central Antarctica, *Earth Planet. Sci. Lett.*, 293, 359–367, doi:10.1016/j.epsl.2010.03.003, 2010. 17776, 17778, 17788, 17789

Constraining firm diffusivity

C. M. Trudinger et al.

Title Page

Abstract

Introduction

Conclusions

References

Tables

Figures

I◀

▶I

◀

▶

Back

Close

Full Screen / Esc

Printer-friendly Version

Interactive Discussion



- Smith, A. M., Levchencko, V. A., Etheridge, D. M., Lowe, D. C., Hua, Q., Trudinger, C. M., Zoppi, U., and Elcheikh, A.: In search of in-situ radiocarbon in Law Dome ice and firn, *Nucl. Instr. Meth. B*, 172, 610–622, 2000. 17786
- 5 Sowers, T., Bernard, S., Aballain, O., Chappellaz, J., Barnola, J., and Marik, T.: Records of the $\delta^{13}\text{C}$ of atmospheric CH_4 over the last 2 centuries as recorded in Antarctic snow and ice, *Global Biogeochem. Cy.*, 19, GB2002, doi:10.1029/2004GB002408, 2005. 17787
- Sturrock, G. A., Etheridge, D. M., Trudinger, C. M., Fraser, P. J., and Smith, A. M.: Atmospheric histories of halocarbons from analysis of Antarctic firn air: Major Montreal Protocol species, *J. Geophys. Res.*, 107, 4765, doi:10.1029/2002JD002548, 2002. 17786, 17799
- 10 Trudinger, C. M.: The carbon cycle over the last 1000 years inferred from inversion of ice core data, PhD thesis, Monash University, available at: http://www.cmar.csiro.au/e-print/open/trudinger_2001a0.htm, 2000. 17778, 17788
- Trudinger, C. M., Enting, I. G., Etheridge, D. M., Francey, R. J., Levchenko, V. A., Steele, L. P., Raynaud, D., and Arnaud, L.: Modeling air movement and bubble trapping in firn, *J. Geophys. Res.*, 102, 6747–6763, 1997. 17776, 17777, 17778, 17785, 17786, 17788, 17789, 17798
- 15 Trudinger, C. M., Etheridge, D. M., Rayner, P. J., Enting, I. G., Sturrock, G. A., and Langenfelds, R. L.: Reconstructing atmospheric histories from measurements of air composition in firn, *J. Geophys. Res.*, 107, 4780, doi:10.1029/2002JD002545, 2002. 17777, 17786, 17788, 17793, 17799
- 20 Witrant, E., Martinerie, P., Hogan, C., Laube, J. C., Kawamura, K., Capron, E., Montzka, S. A., Dlugokencky, E. J., Etheridge, D., Blunier, T., and Sturges, W. T.: A new multi-gas constrained model of trace gas non-homogeneous transport in firn: evaluation and behavior at eleven polar sites, *Atmos. Chem. Phys. Discuss.*, 11, 23029–23080, doi:10.5194/acpd-11-23029-2011, 2011. 17776, 17787
- 25 Wolberg, G. and Alf, I.: An energy-minimization framework for monotonic cubic spline interpolation, *J. Comput. Appl. Math.*, 143, 145–188, 2002. 17780

Constraining firm diffusivity

C. M. Trudinger et al.

Title Page

Abstract

Introduction

Conclusions

References

Tables

Figures

◀

▶

◀

▶

Back

Close

Full Screen / Esc

Printer-friendly Version

Interactive Discussion



Table 1. Site characteristics.

| Site | Date sampled | Accumulation rate $\text{kg m}^{-2} \text{yr}^{-1}$ | Temperature $^{\circ}\text{C}$ | Pressure hPa | Lock-in depth m |
|------------|-------------------|--------------------------------------------------------|-----------------------------------|-----------------|--------------------|
| NEEM | Jul 2008 | 198.8 | −28.9 | 745 | 63 |
| DE08-2 | Jan 1993 | 1100 | −19 | 850 | 73 |
| DSSW20K | Jan 1998 | 150 | −20.7 | 850 | 43 |
| South Pole | Jan 1995 and 2011 | 74 | −49 | 681.5 | 114 |

Constraining firm diffusivity

C. M. Trudinger et al.

[Title Page](#)[Abstract](#)[Introduction](#)[Conclusions](#)[References](#)[Tables](#)[Figures](#)[◀](#)[▶](#)[◀](#)[▶](#)[Back](#)[Close](#)[Full Screen / Esc](#)[Printer-friendly Version](#)[Interactive Discussion](#)**Table 2.** Subsets of tracers used for calibration of diffusivity at NEEM (pseudo and real observations), where the name reflects the number of tracers used.

| Subset | Tracers |
|--------|-------------------------------------------------------------------------------------------------------------------------------------------------------------|
| Two | $\delta^{15}\text{N}_2$, CH_4 |
| Three | $\delta^{15}\text{N}_2$, CH_4 , SF_6 |
| Four | $\delta^{15}\text{N}_2$, CH_4 , SF_6 , HFC-134a |
| Five | $\delta^{15}\text{N}_2$, CH_4 , SF_6 , HFC-134a, CH_3CCl_3 |
| Ten | $\delta^{15}\text{N}_2$, CH_4 , SF_6 , HFC-134a, CH_3CCl_3 , CO_2 , CFC-11, CFC-12, CFC-113, $^{14}\text{CO}_2$ |

Constraining firm diffusivity

C. M. Trudinger et al.

Table 3. Weighted RMS mismatch of modelled concentrations from observations and from the truth for each tracer for each of the five Subsets in Table 2 and TenDC (see Sect. 3.8). Modelled concentrations are for the case with lowest Φ for each experiment. The top half of the table is for Synthetic A calculations, and the bottom half for Synthetic B. Numbers in bold are for tracers that were fitted for that particular Subset. As well as RMS mismatch for each tracer, we also show the RMS mismatch for all ten tracers together (All), and the RMS mismatch for only those tracers that were fitted in that experiment (Fitted). Data uncertainties are used for weights in the cost function, and we use Synthetic A data uncertainties as weights for the mismatch from the truth for Synthetic B concentrations to allow better comparison with Synthetic A results. The first column of numbers shows the RMS mismatch of the true solution from the noisy observations weighted by the data uncertainties.

| Synthetic A | Truth | Mismatch from observations, Φ_A | | | | | | Mismatch from truth, Φ_{At} | | | | | |
|----------------------------------|-------|--------------------------------------|-------------|-------------|-------------|-------------|-------------|----------------------------------|-------------|-------------|-------------|-------------|-------------|
| | | Two | Three | Four | Five | Ten | TenDC | Two | Three | Four | Five | Ten | TenDC |
| CO ₂ | 1.00 | 2.98 | 1.36 | 1.04 | 1.00 | 1.06 | 1.05 | 2.74 | 0.67 | 0.33 | 0.38 | 0.36 | 0.33 |
| CH ₄ | 1.00 | 0.77 | 0.93 | 0.92 | 1.04 | 0.93 | 0.94 | 0.74 | 0.61 | 0.53 | 0.73 | 0.50 | 0.41 |
| SF ₆ | 1.00 | 5.55 | 1.04 | 0.82 | 0.87 | 1.05 | 0.92 | 5.15 | 1.11 | 0.32 | 0.29 | 0.37 | 0.50 |
| CFC-11 | 1.00 | 2.16 | 1.17 | 1.00 | 1.03 | 0.98 | 0.90 | 1.98 | 0.70 | 0.31 | 0.31 | 0.28 | 0.43 |
| CFC-12 | 1.00 | 2.23 | 1.30 | 1.12 | 1.09 | 1.14 | 1.13 | 1.88 | 0.68 | 0.31 | 0.32 | 0.30 | 0.29 |
| CFC-113 | 1.00 | 3.64 | 1.30 | 1.08 | 1.16 | 1.07 | 1.00 | 3.21 | 0.92 | 0.28 | 0.32 | 0.33 | 0.38 |
| HFC-134a | 1.00 | 8.44 | 2.05 | 1.03 | 0.99 | 1.24 | 1.02 | 8.41 | 1.59 | 0.41 | 0.33 | 0.51 | 0.50 |
| CH ₃ CCl ₃ | 1.00 | 9.23 | 2.41 | 1.25 | 1.04 | 1.09 | 1.23 | 9.20 | 2.19 | 0.67 | 0.50 | 0.70 | 0.65 |
| ¹⁴ CO ₂ | 1.00 | 1.17 | 1.09 | 1.05 | 1.11 | 0.73 | 0.73 | 0.80 | 0.28 | 0.45 | 0.74 | 0.63 | 0.60 |
| $\delta^{15}\text{N}_2$ | 1.00 | 0.93 | 0.95 | 0.97 | 0.97 | 0.99 | 1.00 | 0.23 | 0.11 | 0.11 | 0.12 | 0.10 | 0.09 |
| All | 1.00 | 4.71 | 1.44 | 1.03 | 1.03 | 1.03 | 1.00 | 4.57 | 1.06 | 0.40 | 0.45 | 0.44 | 0.44 |
| Fitted | – | 0.86 | 0.97 | 0.93 | 0.99 | 1.03 | 1.00 | 0.49 | 0.61 | 0.34 | 0.39 | 0.44 | 0.44 |
| Synthetic B | Truth | Mismatch from observations, Φ_B | | | | | | Mismatch from truth, Φ_{Bt} | | | | | |
| | | Two | Three | Four | Five | Ten | TenDC | Two | Three | Four | Five | Ten | TenDC |
| CO ₂ | 0.55 | 0.88 | 0.60 | 0.57 | 0.63 | 0.58 | 0.55 | 2.37 | 1.20 | 0.92 | 1.31 | 1.15 | 1.32 |
| CH ₄ | 0.53 | 0.50 | 0.51 | 0.50 | 0.50 | 0.49 | 0.51 | 1.81 | 1.18 | 1.12 | 1.38 | 1.33 | 1.29 |
| SF ₆ | 0.69 | 1.46 | 0.71 | 0.73 | 0.74 | 0.73 | 0.71 | 3.84 | 1.58 | 1.09 | 1.50 | 1.19 | 1.37 |
| CFC-11 | 1.15 | 1.38 | 1.12 | 1.12 | 1.14 | 1.18 | 1.02 | 1.78 | 0.97 | 0.69 | 1.27 | 1.13 | 2.13 |
| CFC-12 | 0.48 | 0.61 | 0.54 | 0.54 | 0.59 | 0.52 | 0.47 | 1.95 | 1.01 | 0.72 | 1.30 | 1.15 | 1.75 |
| CFC-113 | 0.63 | 1.11 | 0.76 | 0.74 | 0.87 | 0.77 | 0.75 | 3.03 | 1.36 | 1.04 | 2.02 | 1.59 | 1.85 |
| HFC-134a | 0.32 | 1.55 | 0.97 | 0.50 | 0.45 | 0.45 | 0.45 | 5.47 | 2.32 | 1.44 | 1.21 | 1.04 | 1.35 |
| CH ₃ CCl ₃ | 0.64 | 2.12 | 0.82 | 0.81 | 0.58 | 0.62 | 0.60 | 6.72 | 2.44 | 1.57 | 0.82 | 1.08 | 1.10 |
| ¹⁴ CO ₂ | 1.70 | 1.65 | 1.72 | 1.68 | 1.59 | 1.50 | 1.49 | 2.17 | 2.00 | 1.55 | 1.63 | 1.50 | 1.87 |
| $\delta^{15}\text{N}_2$ | 1.01 | 0.72 | 0.84 | 0.87 | 0.85 | 0.91 | 0.90 | 0.39 | 0.29 | 0.27 | 0.31 | 0.27 | 0.28 |
| All | 0.81 | 1.28 | 0.87 | 0.83 | 0.82 | 0.80 | 0.77 | 3.46 | 1.57 | 1.11 | 1.34 | 1.19 | 1.51 |
| Fitted | – | 0.62 | 0.70 | 0.68 | 0.65 | 0.80 | 0.77 | 1.10 | 1.02 | 0.98 | 1.04 | 1.19 | 1.51 |

Title Page

Abstract Introduction

Conclusions References

Tables Figures

◀ ▶

◀ ▶

Back Close

Full Screen / Esc

Printer-friendly Version

Interactive Discussion



Constraining firm diffusivity

C. M. Trudinger et al.

Table 4. Weighted RMS mismatch of calculated concentrations for each tracer from the NEEM observations (Φ_N) for the best solution from each of the five Subsets in Table 2 plus Subset Ten with exponential eddy diffusion (denoted TenEddy), Subset Ten with relative diffusion coefficients estimated (TenDC) and TenEddy with relative diffusion coefficients estimated (TenDC Eddy).

| | Two | Three | Four | Five | Ten | TenEddy | TenDC | TenDCEddy |
|----------------------------------|-------------|-------------|-------------|-------------|-------------|-------------|-------------|-------------|
| CO ₂ | 1.37 | 1.04 | 0.86 | 0.90 | 0.72 | 0.76 | 0.76 | 0.62 |
| CH ₄ | 0.46 | 0.50 | 0.56 | 0.67 | 0.65 | 0.61 | 0.59 | 0.58 |
| SF ₆ | 0.69 | 0.43 | 0.45 | 0.51 | 0.61 | 0.56 | 0.29 | 0.33 |
| CFC-11 | 0.94 | 0.95 | 0.96 | 1.01 | 0.95 | 0.94 | 0.95 | 0.94 |
| CFC-12 | 0.92 | 1.06 | 1.02 | 1.15 | 0.85 | 0.85 | 0.52 | 0.55 |
| CFC-113 | 0.70 | 0.71 | 0.67 | 0.76 | 0.53 | 0.55 | 0.51 | 0.49 |
| HFC-134a | 1.44 | 1.33 | 1.01 | 0.93 | 0.95 | 0.95 | 0.93 | 0.99 |
| CH ₃ CCl ₃ | 1.31 | 1.11 | 0.95 | 0.58 | 0.74 | 0.77 | 0.70 | 0.67 |
| ¹⁴ CO ₂ | 0.91 | 0.83 | 0.80 | 1.05 | 0.72 | 0.66 | 0.64 | 0.65 |
| $\delta^{15}\text{N}_2$ | 0.62 | 0.63 | 0.64 | 0.65 | 0.64 | 0.60 | 0.65 | 0.63 |
| All | 0.98 | 0.89 | 0.81 | 0.84 | 0.75 | 0.74 | 0.67 | 0.66 |
| Fitted | 0.55 | 0.53 | 0.67 | 0.66 | 0.75 | 0.74 | 0.67 | 0.66 |

Title Page

Abstract Introduction

Conclusions References

Tables Figures

◀ ▶

◀ ▶

Back Close

Full Screen / Esc

Printer-friendly Version

Interactive Discussion



**Constraining firn
diffusivity**

C. M. Trudinger et al.

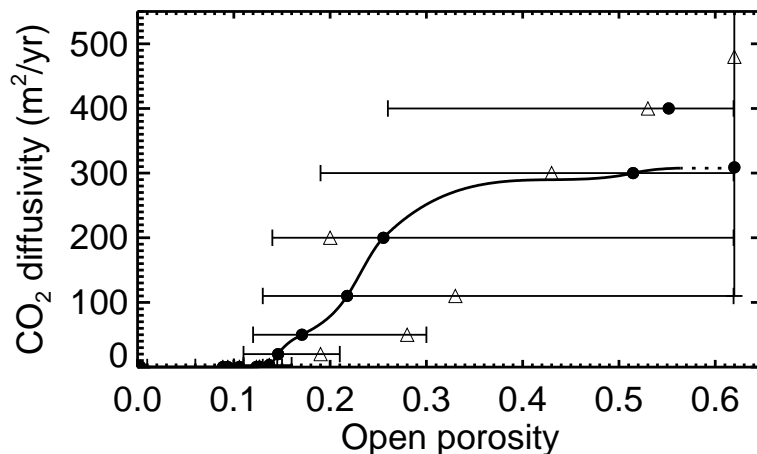


Fig. 1. The error bars show prior ranges for the porosity values and surface diffusivity estimated with the GA. The solid line shows a monotonic smoothing spline fitted to the filled circles (ignoring the point at $400 \text{ m}^2 \text{ yr}^{-1}$ because it is greater than the surface diffusivity, see text). The open triangles show a case with points that do not increase monotonically (so would not be tested in the firn model).

[Title Page](#)[Abstract](#)[Introduction](#)[Conclusions](#)[References](#)[Tables](#)[Figures](#)[◀](#)[▶](#)[◀](#)[▶](#)[Back](#)[Close](#)[Full Screen / Esc](#)[Printer-friendly Version](#)[Interactive Discussion](#)

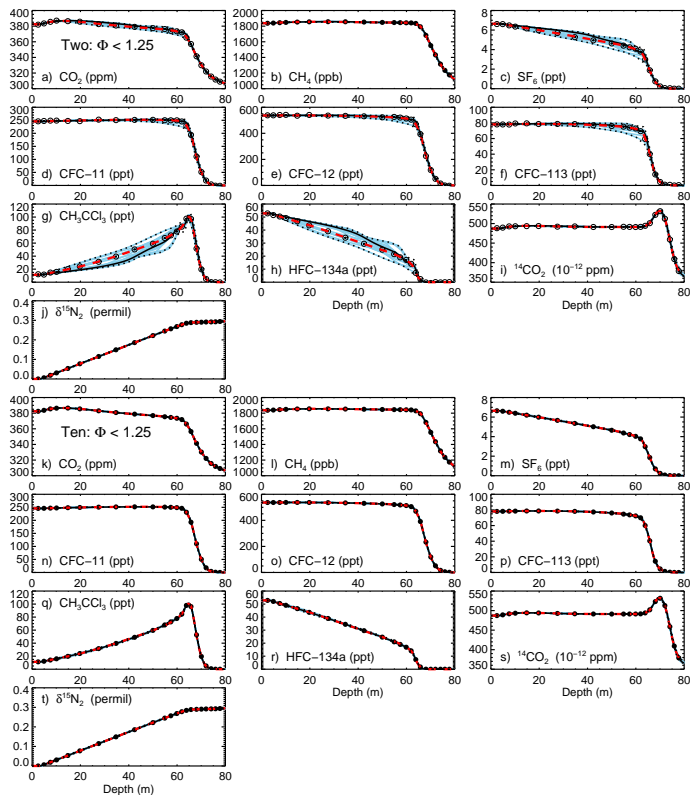


Fig. 2. Modelled concentrations for all ten tracers, where diffusivity was calibrated using Synthetic A observations of only CH_4 and $\delta^{15}\text{N}_2$ (Subset Two) (a–j), and using all ten tracers (Subset Ten) (k–t). The black line is the solution with the lowest Φ_A , dotted lines show upper and lower ranges of all accepted solutions ($\Phi_A < 1.25$), the blue lines are 19 representative solutions and the red dashed line shows the true solution. Observations used to tune diffusivity are shown with filled circles, observations not used in the GA are shown by open circles. Error bars for the observations (1σ) are plotted but are too small to see relative to the symbols.

Constraining firn diffusivity

C. M. Trudinger et al.

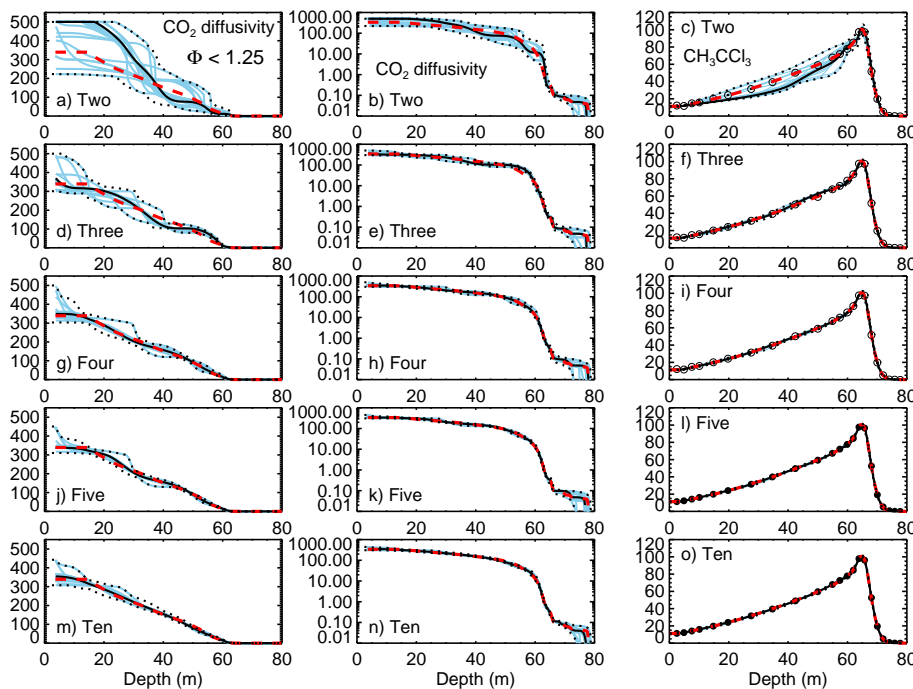


Fig. 3. CO_2 diffusivity profile estimates in $\text{m}^2 \text{yr}^{-1}$ (left column on a linear scale and middle column on a log scale) and calculated CH_3CCl_3 in ppt (right column) from the GA using Synthetic A observations for all five Subsets in Table 2. Line styles are as in Fig. 2 and results are for $\Phi_A < 1.25$.

[Title Page](#)
[Abstract](#)
[Introduction](#)
[Conclusions](#)
[References](#)
[Tables](#)
[Figures](#)
[◀](#)
[▶](#)
[◀](#)
[▶](#)
[Back](#)
[Close](#)
[Full Screen / Esc](#)
[Printer-friendly Version](#)
[Interactive Discussion](#)


Constraining firm diffusivity

C. M. Trudinger et al.

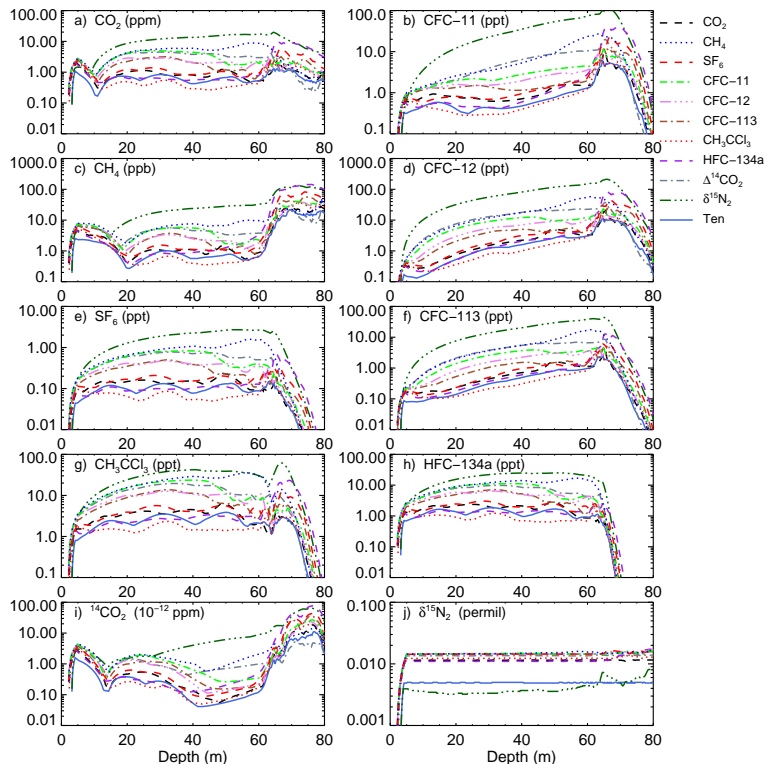


Fig. 4. Range of concentration for all 10 tracers, for all accepted solutions ($\Phi_A < 1.25$) with Synthetic A observations, with each tracer used for calibration on its own and Subset Ten described earlier. Each panel shows the range calculated for one tracer, and each line in that panel corresponds to a different tracer (or Subset Ten) used for calibration.

Title Page

Abstract

Introduction

Conclusions

References

Tables

Figures

◀

▶

◀

▶

Back

Close

Full Screen / Esc

Printer-friendly Version

Interactive Discussion



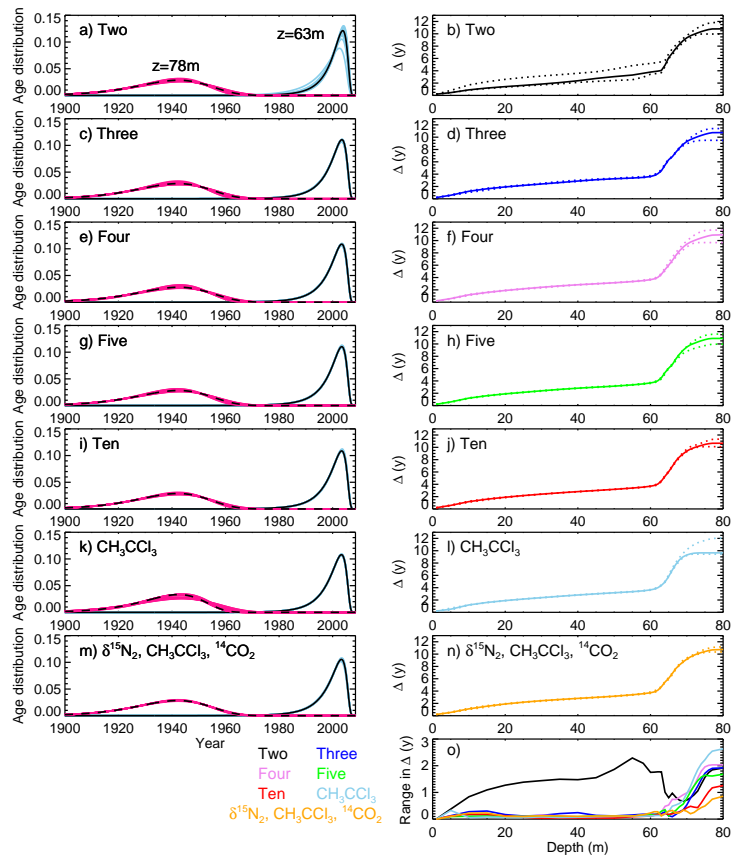


Fig. 5. Panels on the left show age distributions for CO_2 in air at 63 m (solid black lines for the best estimates and blue lines for the other 19 representative estimates with $\Phi_A < 1.25$) and 78 m (dashed black lines for the best estimates and pink lines for the other 19 representative estimates). Cases shown are NEM Synthetic A Subsets Two to Ten, calibration with CH_3CCl_3 alone, and calibration with $\delta^{15}\text{N}_2$, CH_3CCl_3 and $^{14}\text{CO}_2$. Panels on the right show the spectral width versus depth for the same cases. The solid line is the spectral width for the case with lowest Φ_A and the dotted lines show the maximum and minimum values from the ensemble of representative solutions. **(o)** shows the difference between the maximum and minimum values of spectral width for each of the seven cases, using the same colour as that used for each case in the panels above, and also indicated to the left of **(o)**.

Constraining firn diffusivity

C. M. Trudinger et al.

Title Page

Abstract

Introduction

Conclusions

References

Tables

Figures

◀

▶

◀

▶

Back

Close

Full Screen / Esc

Printer-friendly Version

Interactive Discussion

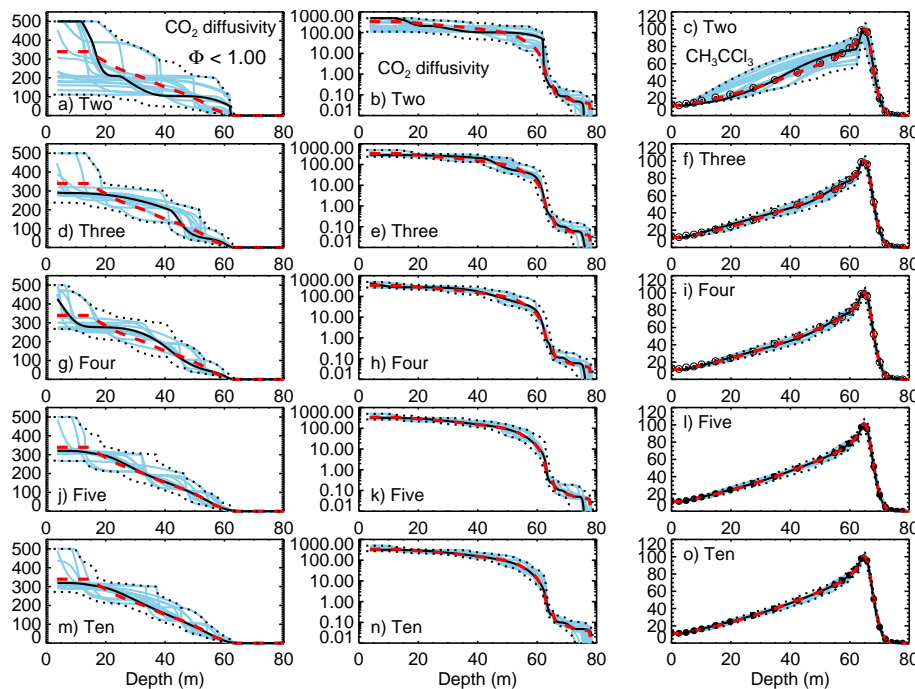


Fig. 6. Depth profiles of CO_2 diffusivity (in $\text{m}^2 \text{yr}^{-1}$) and CH_3CCl_3 (in ppt) from calibration with Subsets of Synthetic B observations. Panels and line styles are as in Fig. 3. Results are for $\Phi_B < 1.0$.

Constraining firm diffusivity

C. M. Trudinger et al.

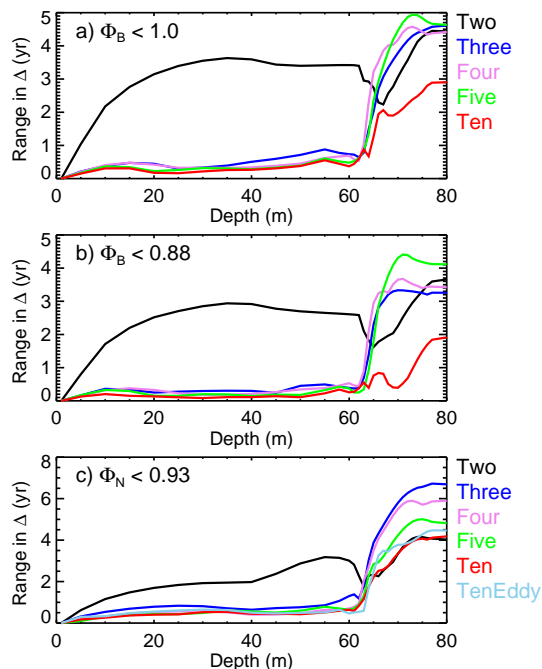


Fig. 7. (a) Range in spectral width versus depth for Synthetic B representative solutions with $\Phi_B < 1.0$ in Subsets Two to Ten, with line colours indicated to the right. (b) Same as in (a) but for $\Phi_B < 0.88$. (c) Range in spectral width versus depth for NEEM representative solutions with $\Phi_N < 0.93$ in Subsets Two to Ten and TenEddy, with line colours indicated to the right.

Title Page

Abstract

Introduction

Conclusions

References

Tables

Figures

◀

▶

◀

▶

Back

Close

Full Screen / Esc

Printer-friendly Version

Interactive Discussion



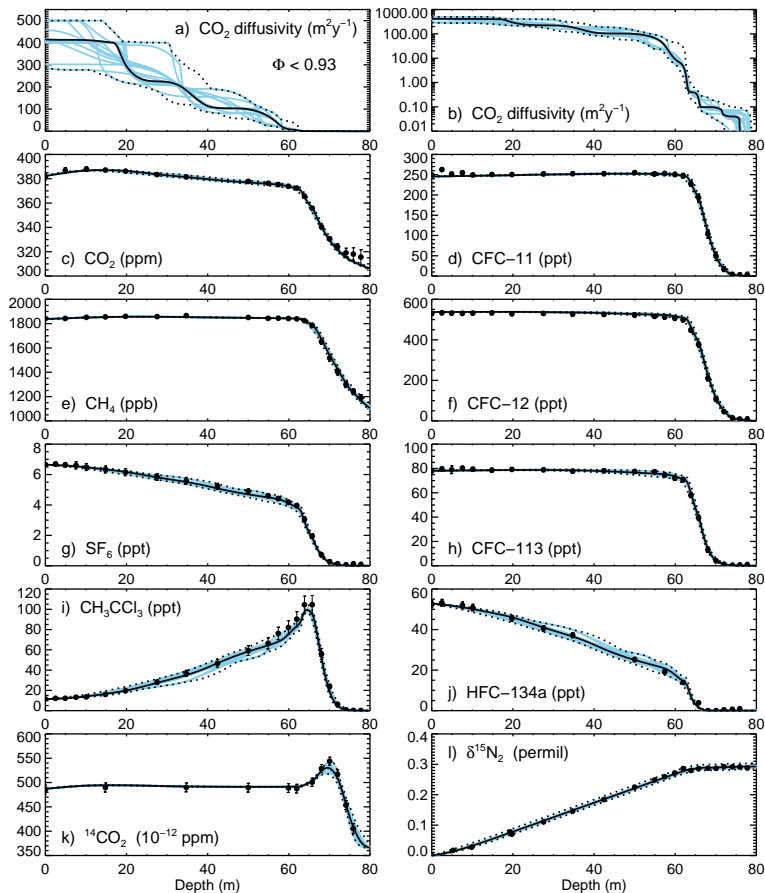


Fig. 8. CO₂ diffusivity and concentration profiles from calibration with all ten NEEM reference tracers from Buizert et al. (2012), with convective mixing modelled by exponentially-decreasing eddy diffusion (TenEddy). Results are for $\Phi_N < 0.93$.

**Constraining fire
diffusivity**

C. M. Trudinger et al.

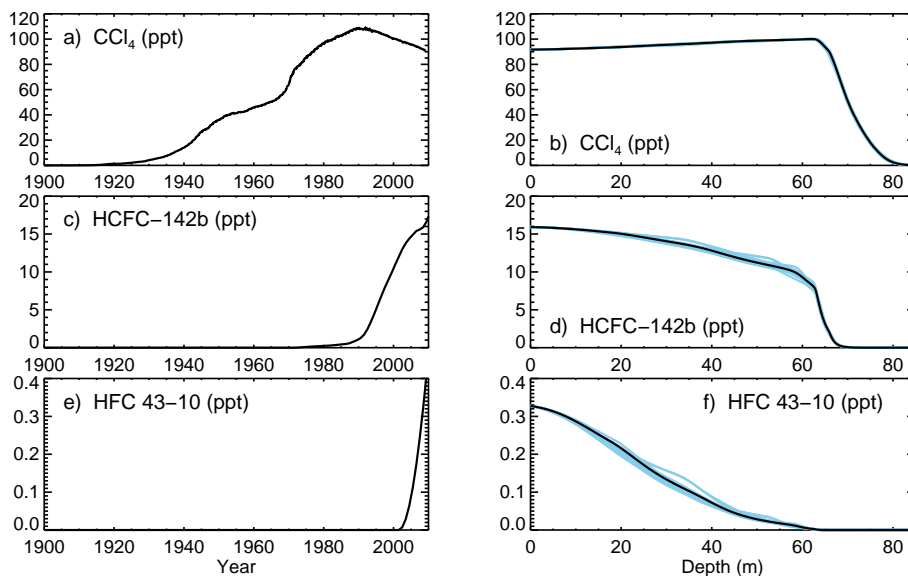


Fig. 9. The left column shows Northern Hemisphere atmospheric histories of CCl_4 , HCFC-142b and HFC-43-10mee (CCl_4 from Martinerie et al. (2009) and HCFC-142b and HFC-43-10mee are Representative Concentration Pathways (Meinshausen et al., 2011) with the RCP3-PD (2.6) from the IMAGE model after 2005). The right column shows modelled firn profiles at NEEM for these tracers, where the black lines show the best case and the blue lines show 19 representative solutions.

[Title Page](#)[Abstract](#)[Introduction](#)[Conclusions](#)[References](#)[Tables](#)[Figures](#)[◀](#)[▶](#)[◀](#)[▶](#)[Back](#)[Close](#)[Full Screen / Esc](#)[Printer-friendly Version](#)[Interactive Discussion](#)

Constraining firm diffusivity

C. M. Trudinger et al.

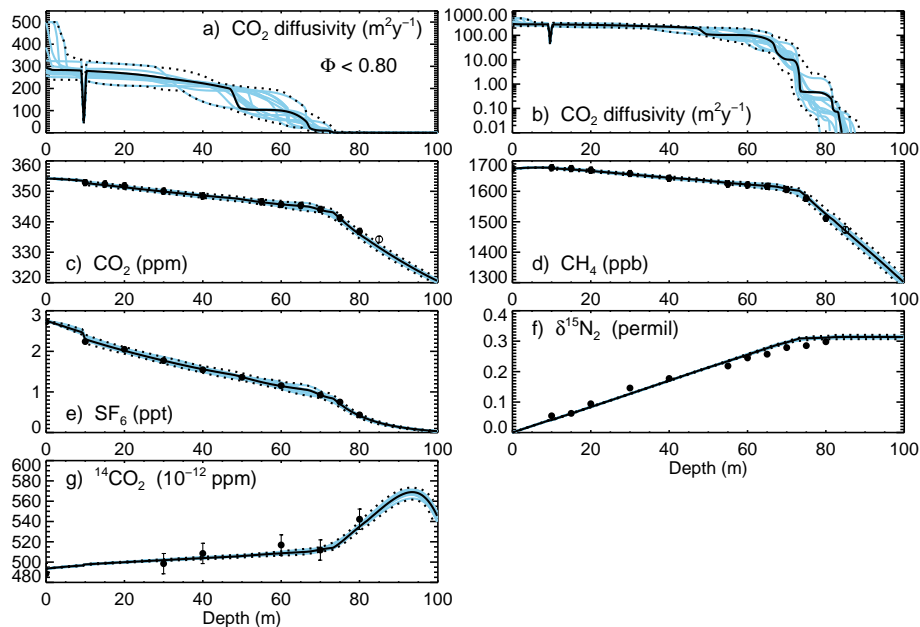


Fig. 10. Diffusivity and tracers at DE08-2 for $\Phi < 0.8$.

Title Page

Abstract

Introduction

Conclusions

References

Tables

Figures

◀

▶

◀

▶

Back

Close

Full Screen / Esc

Printer-friendly Version

Interactive Discussion



Constraining firm diffusivity

C. M. Trudinger et al.

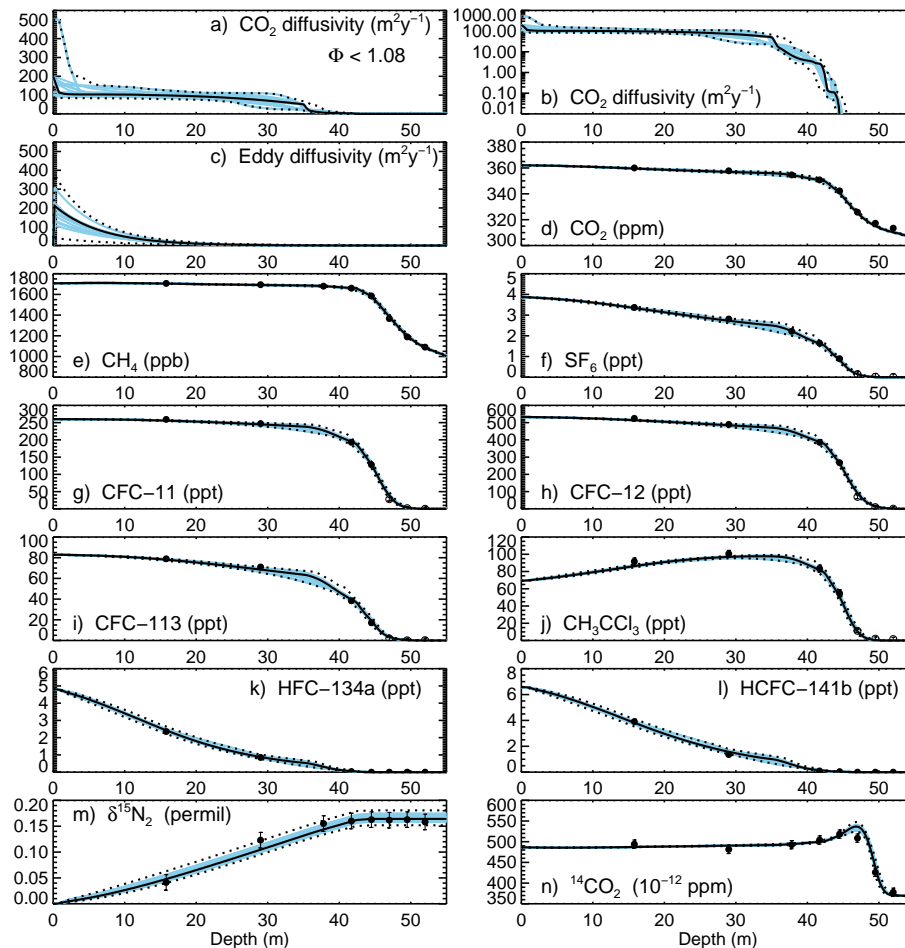


Fig. 11. Diffusivity and tracers at DSSW20K for $\Phi < 1.08$. Solid circles show observations used for calibration, open circles show additional measurements that were not used for calibration.

Constraining firn diffusivity

C. M. Trudinger et al.

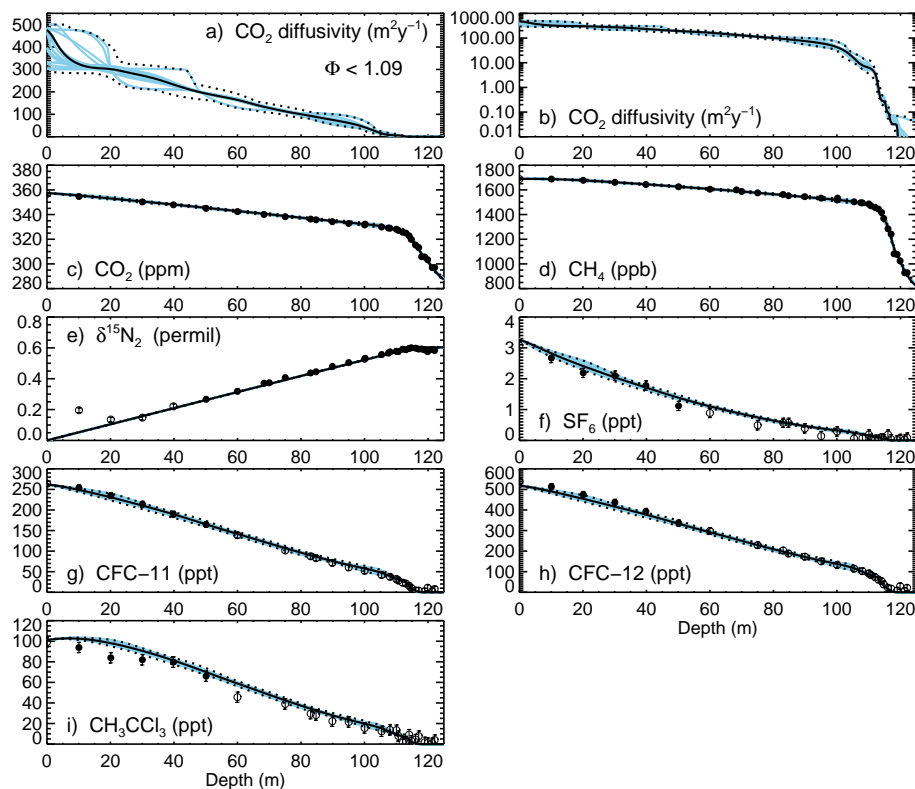


Fig. 12. Diffusivity and tracers at South Pole 1995 for $\Phi < 1.09$. Solid circles show observations used for calibration, open circles show additional measurements that were not used for calibration.

[Title Page](#)
[Abstract](#)
[Introduction](#)
[Conclusions](#)
[References](#)
[Tables](#)
[Figures](#)
[◀](#)
[▶](#)
[◀](#)
[▶](#)
[Back](#)
[Close](#)
[Full Screen / Esc](#)
[Printer-friendly Version](#)
[Interactive Discussion](#)


Constraining firm diffusivity

C. M. Trudinger et al.

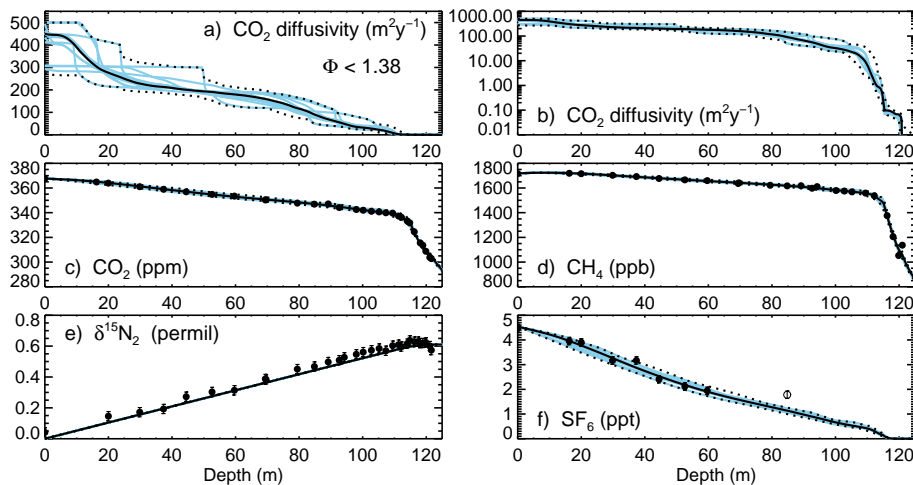


Fig. 13. Diffusivity and tracers at South Pole 2001 for $\Phi < 1.38$. Solid circles show observations used for calibration, open circles show additional measurements that were not used for calibration.

Title Page

Abstract

Introduction

Conclusions

References

Tables

Figures

◀

▶

◀

▶

Back

Close

Full Screen / Esc

Printer-friendly Version

Interactive Discussion



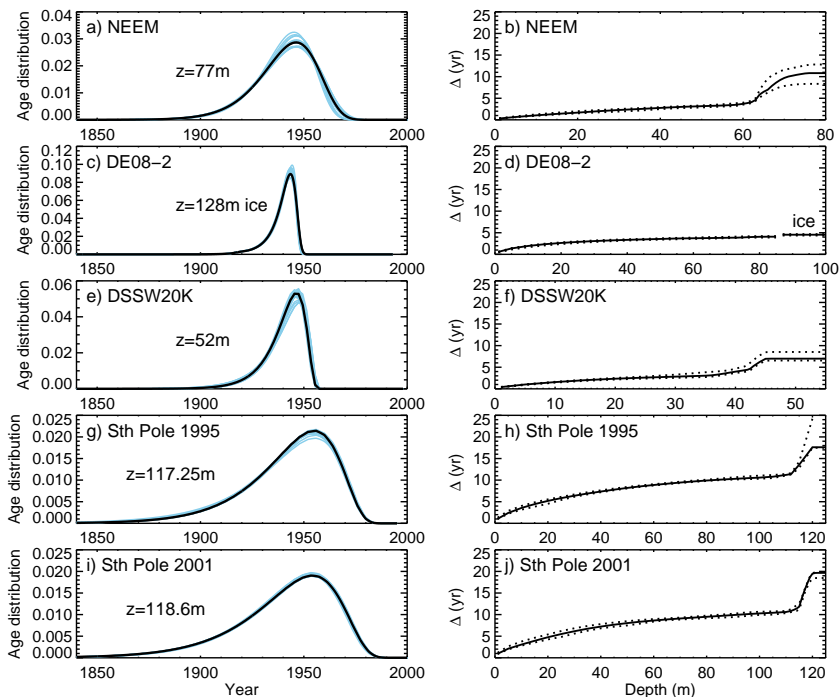


Fig. 14. Plots on the left show CO_2 age distributions for NEEM, DE08-2, DSSW20K, South Pole 1995 and South Pole 2001 corresponding to CO_2 mean ages of 1940. The black lines show the best solution in each case (corresponding to the case with closest match to the reference tracers), and the blue lines show results from 19 representative solutions with diffusivity and other model parameters within the 68 % confidence interval for each site. Plots on the right show variation with depth of the spectral width of the CO_2 age distributions, Δ . The black solid lines are the best case and the dotted lines show the upper and lower ranges of estimates from the 19 representative solutions corresponding to confidence intervals of 68 %. The age distribution for DE08-2 is for air trapped in bubbles in ice at 128 m, and the spectral width plot shows values for the firn to 85 m then ice below this. All other cases are for firn air only.

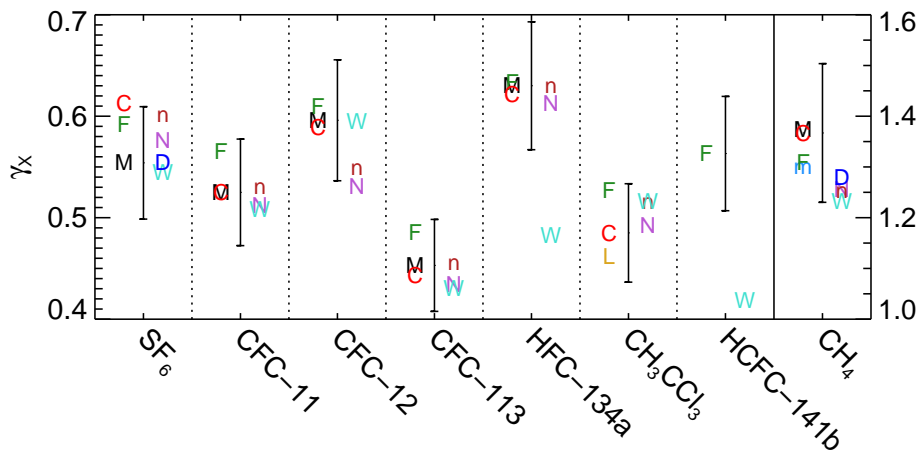


Fig. 15. Relative diffusion coefficients, γ_X , for eight tracers. The error bars indicate $\pm 10\%$ around the Matsunaga et al. (1993, 1998, 2002) values (or Chen and Othmer (1962) for CH_3CCl_3 and Fuller et al. (1966) for HCFC-141b where Matsunaga et al. (1993, 1998, 2002) values are not available). The letters to the left of the error bars are measured or empirical estimates of γ_X , with M = Matsunaga et al. (1993, 1998, 2002), F = Fuller et al. (1966), C = Chen and Othmer (1962), L = Lugg (1968) and m = Marrero and Mason (1972). The letters to the right are estimates from our GA calibrations for different firn sites: N = NEEM with a well mixed layer, n = NEEM with exponential eddy diffusion, D = DE08-2 and W = DSSW20K. All values are adjusted to apply to temperature of 244.25 K. The right axis applies to CH_4 and the left axis applies to all other tracers.

Constraining firn diffusivity

C. M. Trudinger et al.

| | |
|--------------------------|--------------|
| Title Page | |
| Abstract | Introduction |
| Conclusions | References |
| Tables | Figures |
| ◀ | ▶ |
| ◀ | ▶ |
| Back | Close |
| Full Screen / Esc | |
| Printer-friendly Version | |
| Interactive Discussion | |

